Alzheimer's disease linked Aβ42 exerts product feedback inhibition on γ-secretase impairing downstream cell signaling

Zoltowska Katarzyna Marta[1], Das Utpal[2], Lismont Sam[1], Enzlein Thomas[1,3], Maesako Masato[4], Houser Mei CQ[4], Franco María Luisa[5], Gomes Moreira Diana[1], Karachentsev Dmitry[2], Becker Ann[2], Hopf Carsten[3,6,7], Vilar Marçal[5], Berezovska Oksana[4], Mobley William[2*], Chávez-Gutiérrez Lucía[1,*]

[1]VIB-KU Leuven Center for Brain & Disease Research, VIB, Leuven, Belgium

[2]Department of Neurosciences, University of California San Diego, La Jolla, CA, United States of America

[3]Center for Mass Spectrometry and Optical Spectroscopy (CeMOS), Mannheim University of Applied Sciences, Mannheim, Germany

[4]Department of Neurology, Massachusetts General Hospital/Harvard Medical School, Charlestown, MA, United States of America

[5]Molecular Basis of Neurodegeneration Unit, Institute of Biomedicine of València (IBV-CSIC), València, Spain

[6] Medical Faculty, Heidelberg University, Heidelberg, Germany

[7] Mannheim Center for Translational Neuroscience (MCTN), Medical Faculty Mannheim, Heidelberg University, Heidelberg, Germany

* corresponding author

Corresponding authors:

Lucía Chávez-Gutiérrez

VIB-KU Leuven Center for Brain & Disease Research

Herestraat 49 bus 602

3000 Leuven, Belgium

Tel.: +32 16 37 69 35

e-mail: lucia.chavezgutierrez@kuleuven.be

Mobley William

University of California, San Diego

School of Medicine

George Palade Labs (GPL) 359

9500 Gilman Drive

La Jolla, CA 92037-0662

Tel.: 858-337-0864

e-mail: wmobley@health.ucsd.edu

KEYWORDS

Alzheimer's disease, gamma-secretase, presenilin, amyloid beta, amyloid toxicity

ABSTRACT

Amyloid β (Aβ) peptides accumulating in the brain are proposed to trigger Alzheimer's disease (AD). However, molecular cascades underlying their toxicity are poorly defined.

Here, we explored a novel hypothesis for Aβ42 toxicity that arises from its proven affinity for γ-secretases. We hypothesized that the reported increases in Aβ42, particularly in the endolysosomal compartment, promote the establishment of a product feedback inhibitory mechanism on γ-secretases, and thereby impair downstream signaling events.

We show that human Aβ42 peptides, but neither murine Aβ42 nor human Aβ17-42 (p3), inhibit γ-secretases and trigger accumulation of unprocessed substrates in neurons, including C-terminal fragments (CTFs) of APP, p75 and pan-cadherin. Moreover, Aβ42 treatment dysregulated cellular homeostasis, as shown by the induction of p75-dependent neuronal death in two distinct cellular systems.

Our findings raise the possibility that pathological elevations in Aβ42 contribute to cellular toxicity via the γ-secretase inhibition, and provide a novel conceptual framework to address Aβ toxicity in the context of γ-secretase-dependent homeostatic signaling.

INTRODUCTION

Γ-secretases are ubiquitously expressed intramembrane proteases best known for their pathogenic roles in Alzheimer's disease (AD) (*1*). Aberrant processing of the amyloid precursor protein (APP) by γ-secretases leads to the production of longer, aggregation-prone amyloid β (Aβ) peptides that contribute to neurodegeneration (*2*).

In addition, γ-secretases process many other membrane proteins, including NOTCH, ERB-B2 receptor tyrosine kinase 4 (ERBB4), N-cadherin (NCAD) and p75 neurotrophin receptor (p75-NTR) (*3, 4*). The processing of multiple substrates links their activity to a broad range of downstream signaling pathways (*5, 6*), including those critical for neuronal structure and function. It is noteworthy that treatment with γ-secretase inhibitors caused cognitive worsening in AD patients (*7*), while genetic inhibition of these enzymes led to neurodegenerative phenotypes in mice (*8-12*). The underlying mechanisms by which deficits in γ-secretase activity impair neuronal function are yet to be defined.

Γ-secretase activity is exerted by a family of highly homologous multimeric proteases composed of presenilin (PSEN1 or PSEN2), nicastrin (NCSTN), anterior pharynx defective 1 (APH1A or B) and presenilin enhancer 2 (PEN2) subunits. The proteolytic activities of these complexes are promoted by the low pH of the endosomal and lysosomal compartments, wherein the amyloidogenic processing of APP occurs (*13*). In the amyloidogenic pathway the proteolytic processing of APP by β-secretase (BACE) releases a soluble APP ectodomain and generates a membrane-bound C-terminal fragment (β-CTF or APP_{C99}) (*14*). APP_{C99} is then sequentially processed within the membrane by γ-secretase complexes **(Figure 1A)** (*15-19*). An initial endopeptidase (ε-) cut releases APP intracellular domain (AICD) into the cytosol and generates a *de novo* substrate (either Aβ49 or Aβ48 peptide) that undergoes successive γ-cleavages until a shortened Aβ peptide is released into the luminal or extracellular environment. The efficiency of the sequential cleavage mechanism (i.e. processivity) defines Aβ length: 37-43 amino acid long peptides, which vary in their aggregation and neurotoxic properties, are generated (*2, 20, 21*). In the non-amyloidogenic pathway APP is cleaved by α- and γ-secretases to generate a spectrum of p3 peptides, which lack the first 1-16 amino acids of Aβ **(Figure 1A)**. Of note, the p3 peptides are not linked to AD pathogenesis (*22-24*) despite their relatively high hydrophobicity and aggregation prone behavior. In fact, mutations promoting the amyloidogenic processing of APP are

linked to AD (*25, 26*), while those favoring the alternative, non-amyloidogenic pathway protect against the disease (*24, 27*).

In familial AD (FAD), mutations in PSENs or in APP/Aβ (i.e. changes impacting both the enzyme and its substrate) promote the generation of longer Aβ peptides, including Aβ42, but also Aβ43 (*28-33*). These peptides accumulate in the brain and are a hallmark of AD, in both familial and sporadic forms. In the latter (SAD), the accumulation of longer, aggregation prone peptides results from their inefficient clearance (*34, 35*). Irrespective of the mechanism, the accumulation of Aβ in the brain begins decades before the onset of clinical symptoms and is proposed to trigger toxic cascades via poorly understood mechanisms (*2*).

Aggregation of Aβ42 into soluble toxic oligomers has been proposed as a prerequisite for its toxicity (*36-39*). However, given the broad spectrum of brain-derived Aβ peptides and their assemblies, it seems plausible that the pleiotropic nature of Aβ actions contribute via a number of mechanisms to AD pathogenesis. Of note, increasing evidence suggests that in addition to Aβ (*2*), its precursor, the 99 amino acid C-terminal fragment (i.e. APP_{C99}) (*40*) also mediates pathogenic mechanisms.

Herein, we explored a novel hypothesis for Aβ42 toxicity that arises from its proven affinity for γ-secretases. We hypothesized that pathological increases in Aβ levels in the AD brain resulted in the establishment of a product feedback inhibitory mechanism, wherein Aβ1-42 competed with membrane-associated substrates for γ-secretase processing. This hypothesis is supported by our reported observations that Aβs with low affinity for γ-secretase, when present at relatively high concentrations, can compete with the longer, higher affinity APP_{C99} substrate for binding and processing by the enzyme (*30*). This hypothetical inhibitory feedback would result in the accumulation of unprocessed γ-secretase substrates and reduced levels of their soluble intracellular domain (ICD) products, possibly disrupting downstream signaling cascades.

To test the hypothesis, we investigated whether Aβ peptides can exert product feedback inhibition on γ-secretase. Our kinetic analyses demonstrate that human Aβ1-42 inhibits γ-secretase-mediated processing of APP_{C99} and other substrates. Strikingly, neither murine Aβ1-42 nor human p3 (17-42 amino acids in Aβ) peptides exerted inhibition under similar conditions. We also show that human Aβ1-42-mediated inhibition of γ-secretase activity results in the accumulation of unprocessed

CTFs of APP, p75 and pan-cadherins. To evaluate the impact of the Aβ-driven inhibition on cellular signaling, we analyzed p75-dependent activation of caspase 3 in basal forebrain cholinergic neurons (BFCNs) and PC12 cells. These analyses demonstrate that, as seen for γ-secretase inhibitors (*41*), Aβ1-42 potentiates this marker of apoptosis. Our findings thus point to an entirely novel and selective role for the Aβ42 peptide, and raise the intriguing possibility that compromised γ-secretase activity against the CTFs of APP and/or other neuronal substrates contributes to the pathogenesis of AD.

RESULTS

Aβ1-42 inhibits γ-secretase-mediated proteolysis of APP_{C99}

Aβ peptides displaying a relatively low affinity for γ-secretase, when present at high concentrations, can compete with the higher affinity APP_{C99} substrate for binding to the enzyme (*30*). Based on this observation, we hypothesized that increments in concentration of the AD-linked Aβ42 peptides may promote the establishment of a product feedback mechanism that involves the formation of 'non-productive' enzyme-Aβ42 complexes and results in the inhibition of γ-secretases. The Aβ42-mediated inhibition would lead to the accumulation of unprocessed γ-secretase substrates and decreased production of their intracellular domains, both possibly contributing to dysregulated downstream signaling.

As a first step, we investigated the effects of human Aβ1-42 (from now on referred to as Aβ42) on the processing of APP_{C99} in well-controlled kinetic analyses **(Figure 1B)** (*30*). We incubated purified (wild type) γ-secretase enzyme with purified APP_{C99}-3xFLAG substrate at the K_M or saturating concentrations (0.4 μM and 1.2 μM, respectively) in the presence of human Aβ42 peptides at concentrations ranging from 0.5 μM to 10 μM. We then analyzed *de novo* generation of AICD-3xFLAG by quantitative western blotting **(Supplementary figure 1)**. Methanol:chloroform extraction was performed to remove the excess of unprocessed substrates, the high levels of which could preclude quantitative analysis of ICDs. The analysis demonstrated that human Aβ42 inhibited γ-secretase-mediated proteolysis of APP_{C99} in a dose dependent manner. The more pronounced peptide-driven inhibition at the lower substrate concentration (IC_{50}=1.3 μM vs 3.6 μM for 0.4 and 1.2 μM APP_{C99}, respectively) is consistent with a mechanism in which Aβ42 competes with the substrate for the enzyme.

In addition, mass spectrometry analyses of the proteolytic reactions showed that Aβ42 inhibited the generation of both AICD product types ($AICD_{50-99}$ and $AICD_{49-99}$) **(Figure 1C)**, indicating that Aβ42 inhibits both γ-secretase product lines. Next, we tested whether human Aβ42 exerts inhibition on all members of the γ-secretase family – i.e. irrespective of the type of PSEN (1 vs 2) and APH1 (A vs B) subunits **(Figure 1D)**. Quantitative western blotting analysis revealed a marked inhibition of total AICD production by all types of γ-secretases in the presence of 3 μM human Aβ42. These findings support a competitive mechanism wherein low-affinity substrates (normally acting as products) are able to re-associate with the protease and inhibit the processing of substrates when present at relatively high concentrations.

To gain further insight into the inhibitory mechanism, we investigated γ-secretase mediated processing of Aβ42 to Aβ38 under the conditions used to examine APP_{C99}, using the latter as a positive control **(Figure 1E)**. The results showed that, despite the use of relatively high concentrations of Aβ42 (10 μM), this peptide was not converted into Aβ38, while proteolytic reactions using APP_{C99} (1.5 μM) resulted in the generation of Aβ38 (0.5-1 nM). We also tested whether Aβ42 served as a substrate in a native-like environment, i.e. detergent resistant membranes (DRMs) **(Figure 1E)** (*30, 42*). As in detergent conditions, Aβ42 was barely converted into Aβ38. Of note, we have shown that γ-secretase processes Aβ43 into Aβ40 under similar conditions, even when this peptide was added at much lower concentrations (0.5-1 μM) (*30*). These observations indicate that exogenous Aβ42, in contrast to Aβ43, does not act as a substrate in these conditions. Accordingly, Aβ42-driven inhibition of γ-secretases supports formation of non-productive enzyme-substrate (E-S) like complexes as an underlying mechanism. Nevertheless, a scenario wherein Aβ42 interacts with APP_{C99} to reduce the amount of free APP_{C99} substrate available for the enzymatic cleavage was not excluded by these data.

Whether or not the inhibitory effects of Aβ42 on γ-secretase were reversible was also evaluated. To this end, using a high affinity anti-NCSTN nanobody we conjugated purified γ-secretase complexes to beads and incubated the 'enzyme-attached' beads with 0.4 μM APP_{C99}, in the absence or presence of 3 μM Aβ42, for 40 minutes at 37°C. This concentration of peptide substantially inhibited AICD generation **(Figure 1B)**. As a control, 10 μM γ-secretase inhibitor X (GSI, Inh X) was included. After incubation we collected the supernatants, washed the beads in assay buffer and re-incubated them with

0.4 μM APP_{C99} for 40 minutes at 37ºC. Analysis of the levels of the *de novo* generated AICD products in the supernatant fractions collected after the first incubation indicated that Aβ42 inhibition of γ-secretase was fully reversible **(Figure 1F)**. Collectively, our analyses support a model wherein Aβ42 forms non-productive E-S like complex with γ-secretase and its binding is reversible.

The N- and C-termini of Aβ play key roles in the inhibition of γ-secretase activity

We next investigated the structure-function relationships relevant for the Aβ42-driven inhibitory mechanism. The effects of mouse/rat (murine) Aβ42 and N-terminally truncated human Aβx-42 (11-42 and 17-42) peptides on γ-secretases activity were examined in cell-free assays using peptide concentrations ranging from 0.5 μM to 10 μM **(Figure 2A-C)**. Quantification of the *de novo* AICD product levels showed that murine Aβ42 maximally inhibits γ-secretases activity by ~20% **(Figure 2A)**. Because three amino acids in the N-terminal domain (R5G, Y10F and H13R) differentiate human and murine Aβ1-42 peptides **(Figure 1A)**, the differences in inhibition thus defined the N-terminal domain of Aβ as contributing to the inhibitory mechanism. The analyses of other naturally occurring N-terminally truncated Aβx-42 peptides, generated by β-secretase (alternative) cleavage at position 11 or by α-secretase cut at position 17 in the Aβ sequence, demonstrated that relative to Aβ42, the truncated peptides presented reduced inhibitory potencies. The IC_{50} values for Aβ11-42 were reduced 1.79- and 1.31- fold (K_M and saturating substrate concentrations, respectively), relative to Aβ42 **(Figure 2B, Supplementary Table 1)**, while the larger N-terminal truncation (of residues 1-16) abolished the inhibitory effect **(Figure 2C)**. Collectively, these data assign a defining role for the N-terminal region of Aβ in mediating the inhibition of γ-secretase activity.

We next tested whether longer Aβ peptides (>Aβ42), that form more stable interactions with the protease (*30*), also inhibit γ-secretase activity. In addition, we investigated whether shortening of the C-terminus diminishes the inhibitory properties. To this end, we evaluated a series of naturally occurring Aβ1-x peptides, ranging from 37 to 43 amino acids in length, at 1 μM final concentration, for their effects on γ-secretase proteolysis of APP_{C99} **(Figure 2D)**. In these experiments reducing the DMSO (vehicle) concentration to 0.2% was attended by enhanced Aβ-mediated inhibition by ~1.7 fold relative to the conditions shown in Figure 1B. We speculate that increased Aβ potency under these conditions is

explained by a modest but measurable reduction in proteolysis by the higher concentration of DMSO used in Figure 1 assays (*43*). Relative to Aβ42, shorter Aβ species exerted progressively less or no inhibition on the *de novo* generation of AICD. Of note, peptides longer than Aβ42 serve as a substrate of γ-secretases in these conditions and might be converted into shorter, less potent species (*30*). Taken together, the data strengthen the conclusion that human Aβ42 inhibits γ-secretases and indicate that both Aβ C- and N-termini modulate the inhibitory mechanism.

Human Aβ42 inhibits endogenous γ-secretase activity in neurons

The consistent inhibitory properties of human Aβ42 demonstrated in cell-free systems motivated cellular studies to address the effects of this peptide on the processing of γ-secretase substrates in cellular context. We applied an established cell-based γ-secretase activity assay to test *in situ* the protease activity in primary mouse neurons (*44, 45*) **(Figure 3A)**. This assay utilizes an APP_{C99}-based fluorescent substrate (the C99 Y-T biosensor) to probe γ-secretase activity *in situ*. This biosensor comprises APP_{C99} fused at the C-terminus with YPet, followed by a linker, Turquoise-GL and a membrane anchoring domain to stabilize the probe in the membrane. The cleavage of the APP_{C99}-based probe by endogenous γ-secretases extends the distance between YPet and Turquoise-GL, and therefore results in a decrease in the efficiency of Förster resonance energy transfer (FRET) for this pair. The ratiometric nature of the reporter, and its independence of α- and β-secretase activity and cellular degradation mechanisms, allow quantitative analysis of γ-secretase activity in living cells.

To determine the effects of Aβ or p3 peptides on γ-secretase, we treated mouse primary neurons with human Aβ42, p3, GSI (1 μM DAPT) or vehicle (DMSO) for 24h and performed FRET analysis **(Figure 3B-C)**. While p3 peptides did not affect the FRET signal, significant increases in FRET efficiency (i.e. increased proximity between YPet and Turquoise-GL) in cells treated with human Aβ42 or GSI, relative to vehicle treated cultures, indicated increments in the levels of the full-length (uncleaved) fluorescent substrate, and thus reduced γ-secretase activity. These findings thus provided, in a cellular context, quantitative evidence supporting the inhibition of endogenous γ-secretases by human Aβ42, but not p3 17-42 peptides.

Aβ42 treatment leads to the accumulation of APP C-terminal fragments in neuronal cell lines and human neurons

We then reasoned that human Aβ42-driven inhibition of γ-secretase activity would lead to the accumulation of unprocessed γ-secretase substrates in cells: APP-CTFs in the case of APP. To test this possibility, we treated human neuroblastoma SH-SY5Y, rat pheochromocytoma PC12 and human neural progenitor cells (ReNcell VM) with either human Aβ42 or p3 17-42 at 1 μM or 2.5 μM final concentrations, and analyzed the levels of APP-CTFs and full-length APP (APP-FL) by western blotting **(Figure 4A-C)**. Treatment with GSI (InhX) at 2 μM was included as a positive control, and APP-FL amounts were used to normalize for the APP substrate availability. Human Aβ42 treatment increased the APP-CTF/FL ratio, a read-out of γ-secretase activity. In contrast, treatment with p3 peptide had no effect. To control for overall cellular toxicity of Aβ42 peptides, we performed two cellular toxicity assays **(Figure 4D-E)**. In the first, we quantified the activity of lactate dehydrogenase (LDH) released by cells into medium upon plasma membrane damage. In the second, we detected cellular ATP as a reporter of viability. There was no significant change in these measures in response to addition for 24h of Aβ42 (1 μM), p3 17-42 (1 μM), or GSI (2 μM) on SH-SY5Y cells.

To ask if the effects of Aβ42 would be registered in wild type human neurons we examined neurons derived from induced pluripotent stem cell (iPSC) and treated with human or murine Aβ42, p3 17-42 or human Aβ40 (all at 2.5 μM). Only treatment with human Aβ42 resulted in a significant increase of APP-CTFs **(Figure 4F)**, supporting the inhibitory role of Aβ42.

Aβ peptides derived from biological sources trigger APP C-terminal fragment accumulation

We next asked if Aβ from disease-relevant biological sources would recapitulate the effects of recombinant Aβ42. For these studies we used culture medium conditioned by human iPSC-derived neurons expressing APP wild type or the KM670/671NL (SWE) variant. The APP SWE mutation increases total Aβ production by promoting the amyloidogenic processing of APP. ELISA-based quantification of Aβ content estimated a total concentration in the low nanomolar range (0.5-1 nM). Conditioned medium (WT or SWE) was applied to PC12 cells either directly or after Aβ depletion

(delSWE) using the anti-APP 3D6 (epitope Aβ 1-5) **(Figure 4G)**. After a 24h incubation at 37ºC, the APP-CTF/FL ratio was measured. Cells incubated in control, unconditioned media were used as a reference control. We observed significant increments in the APP-CTF/FL ratio in cells treated with SWE conditioned media, relative to control cells. Aβ immunodepletion from the SWE medium (delSWE-CM) lowered the APP-CTF/FL ratio to the levels observed in the control cells. These data provide evidence that Aβ peptides derived from biological sources induce accumulation of APP-CTFs even when present at low nM concentrations, and thus point to this biological source of Aβ peptides as being far more potent than recombinant Aβ42.

Selective accumulation of Aβ42 in cells leads to increased APP C-terminal fragments

Next, we examined the effects of a broader spectrum of Aβ peptides, presenting different N- and C-termini, on APP-CTF levels in SH-SY5Y cells. In addition, we tested murine Aβ42, which failed to inhibit γ-secretase activity in cell-free assays **(Figure 5A)**. The analysis confirmed a significant ~2.5-fold increase in the APP-CTF/APP-FL ratio in cells treated with human Aβ42 but, intriguingly, none of the other investigated peptides significantly changed APP-CTF levels.

These observations provided evidence that Aβ42 differs from other tested peptides in one or more features that are critical for γ-secretase inhibition in cells. Previous studies have shown that selective cellular uptake of human Aβ42, relative to Aβ40, leading to its concentration in the acidic endolysosomal network (ELN), promotes peptide aggregation into soluble toxic Aβ species (*46-48*). We reasoned that since this compartment is the main locus of γ-secretase activity (*45*), the concentration of Aβ42 in ELN may not only promote its aggregation but also facilitate its inhibitory actions on γ-secretases. To investigate whether the selective accumulation of Aβ42 in ELN, relative to other tested peptides, could explain the differential (cellular) inhibitory profiles of the tested peptides **(Figure 5B)**, we treated PC12 cells with human Aβ40, Aβ42, Aβ43 or p3 17-42, or murine Aβ42 peptides at 1 μM final concentration for 24h, and investigated their intracellular pools by immunostaining with an anti-Aβ/p3 antibody, 4G8 (epitope: 17-23 aa). We found that, unlike other Aβ or p3 peptides, human Aβ42 accumulated in cells. The data is consistent with a model in which selective cellular uptake and/or

intracellular accumulation of Aβ42 distinguishes it from the other examined peptides and explains its unique inhibitory properties in the cellular context**.**

Human Aβ42 peptides inhibit proteolysis of other γ-secretase substrates, beyond APP-CTFs

The Aβ42-mediated inhibition of endogenous γ-secretase activity in cells raises the possibility that Aβ42 would inhibit the processing of γ-secretase substrates beyond APP-CTFs. To address this possibility, we analyzed in cell-free conditions the effects of human Aβ42 on the processing of a purified NOTCH1-based substrate **(Figure 6A)**. We incubated purified γ-secretase and the NOTCH1-based substrate (at 0.4 μM or 1.2 μM concentrations) in the presence of increasing amounts of human Aβ1-42 (ranging from 0.5 μM to 10 μM). Quantification of the *de novo* generated NICD-3xFLAG showed a dose dependent inhibition of γ-secretase proteolysis of NOTCH1 by Aβ42. As for APP_{C99}, the derived IC_{50} values showed that the degree of the inhibition depended on substrate concentration, consistent with a competitive mechanism **(Supplementary Table 1)**. We extended this analysis by assessing the γ-secretase-mediated proteolysis of other substrates (ERBB4-, neurexin- and p75-based) in the presence of 3 μM human Aβ42 **(Figure 6B)**. Quantification of the respective *de novo* generated ICDs revealed that Aβ42 reduced γ-secretase proteolysis of each of these substrates. Mass spectrometry-based analyses of the respective ICDs confirmed the inhibition **(Supplementary figure 2)**.

We next investigated the effects of human Aβ42 on the γ-secretase-mediated processing of pan-cadherin in ReNcell VM cells. Cleavage of cadherins by α-secretase generates a membrane bound CTF, which is a direct substrate of γ-secretases (*49*). As before, we used the PanCad-CTF/FL ratio to estimate the efficiency of the γ-secretase-mediated proteolytic processing **(Figure 6C)**. Human Aβ42 and InhX, but not p3, treatments resulted in significant increments in the PanCad-CTF/FL ratio, demonstrating that Aβ42 inhibits processing of several different γ-secretase substrates. These results suggest that this peptide may be able to generally impact proteolysis of γ-secretases substrates.

In demonstrating that Aβ42 inhibits γ-secretase proteolysis of substrates that are structurally distinct from APP-CTFs, these data point to Aβ42 inhibiting enzyme activity independent of substrate structure. In so doing, they render much less likely the mechanistic possibility considered above, that inhibition is due to interaction with the substrate.

Human Aβ42 driven accumulation of p75-CTF induces markers of neuronal death

The p75 neurotrophin receptor plays a prominent role in neurotrophin signaling. Under certain conditions its C-terminal fragment (p75-CTF, a γ-secretase substrate) modulates cell death (*50, 51*). Previous studies have shown that accumulation of p75-CTF in basal forebrain cholinergic neurons (BFCNs), due to pharmacological inhibition of γ-secretases, triggers apoptosis in a TrkA activity dependent manner (*41*). The proapoptotic action of p75-CTF is prevented by expression of the TrkA receptor for nerve growth factor (NGF), which serves as a co-receptor with p75 (*41*). Similar observations were made in PC12 cells, which model sympathetic neurons. In this case, γ-secretase inhibitors increased apoptosis in TrkA-deficient (PC12nnr5) (*52*), but not in wild type, TrkA expressing cells. These findings provided an experimental system to investigate the effects of Aβ42 mediated inhibition on γ-secretase-mediated signaling in neurons and neuron-like cells.

We tested the impact of Aβ on p75 signaling in wild type and PC12nnr5 cells. We exposed the cells to 1 μM human Aβ42, 1 μM p3, GSI (10 μM compound E) or vehicle (DMSO) for 3 days, and measured apoptosis via immunofluorescence staining for cleaved caspase 3 **(Figure 6D)**. In addition, to assess γ-secretase proteolysis of p75, we measured the p75-CTF/FL ratio in the treated cultures **(Figure 6E)**. Cleaved caspase 3 staining was increased in PC12nnr5 cells treated with GSI or human Aβ42, but not in those exposed to p3 or vehicle (DMSO). Of note, and consistent with past findings (*41*), none of the treatments elicited significant increases in cleaved caspase 3 in wild type PC12 cells that express physiological levels of TrkA. In addition, analysis of the p75-CTF/FL ratio demonstrated higher p75-CTF levels in GSI and Aβ42 treated cells. These results, together with our previous observations, strongly suggest that Aβ42-mediated accumulation of p75-CTFs results in cell death signaling in the absence or near absence of TrkA expression. Our similar studies using BFCNs recapitulated the reported increased cell death under conditions in which both γ-secretase and TrkA activities were inhibited (CE and K252α inhibitor) (*41*), and showed that treatment with 1 μM human Aβ42 mimics the increase in cleaved caspase 3 driven by the GSI **(Figure 6F)**. In conclusion, these results strongly support a novel role for human Aβ42 peptide in the global inhibition of γ-secretase activity and point to this Aβ42-induced mechanism as dysregulating cellular homeostasis.

Aβ42-mediated γ-secretase inhibition is the major mechanism contributing to APP-CTF accumulation in cells

Our data derived from well-controlled, cell-free systems and cell-based assays utilizing a concentration independent (FRET) reporter of γ-secretase activity support a direct impact of Aβ42 peptides on the activity of the enzyme. Of note, these systems are independent of α- and β-secretase cleavages as well as cellular degradation pathway, hence they allow selective and specific analysis of γ-secretase activity. Nevertheless, it is possible that in cells all or some of the aforementioned mechanisms act jointly and converge on the observed increase in APP-CTFs.

To investigate the impact of Aβ42 on α-secretase (ADAM10) and β-secretase (BACE1), the increased expression or activity of which could result in increased APP-CTF levels, we analyzed the levels of soluble APP (sAPP) in conditioned medium collected from SH-SY5Y cells treated with Aβ40 (1 μM), Aβ42 (1 μM), p3 17-42 (1 μM), GSI (InhX, 2 μM) or vehicle DMSO control, as well as the expression of ADAM10 and BACE1 in total cell lysates **(Supplementary figure 3)**. We found no evidence for either increased α-secretase and β-secretase levels or activity. Our analysis actually showed a reduction in sAPP levels in the conditioned medium collected from cells treated with Aβ42. Further studies are required to define whether the sAPP decrease in a consequent of sheddase inhibition.

Next, to evaluate potential γ-secretase independent changes in the degradation of APP-CTF, we assessed the impact of Aβ42 peptides on γ-secretase independent APP-CTF half-life using a well-established cycloheximide (CHX)-based assay. CHX inhibits protein synthesis through blocking translation elongation (*53*). In these experiments, we pre-treated SH-SY5Y cells with either GSI (DAPT, 10 μM) or GSI + Aβ42 (1 μM) for 24h to accumulate APP-CTFs. Next, we added CHX (50 μg/ml) and then collected the cells thereafter at 0h, 1h, 2.5h and 5h. Bafilomycin A1 (200 nM), which de-acidifies lysosomes and compromises degradation, was used as a positive control **(Figure 7A and B)**. Quantitative analysis of the levels of both APP-CTFs and APP-FL over the 5h time-course failed to reveal significant differences between Aβ42 treated cells and controls. As expected, Bafilomycin A1 treatment markedly prolonged the half-life of both proteins **(Figure 7C)**. This study demonstrated the lack of a significant impact of Aβ42 on the half-life of APP-CTFs under the conditions of γ-secretase inhibition. However, we noted increased APP-CTF/FL ratio in GSI + Aβ42 treated cells vs GSI + DMSO

treated cells at zero time point. The additive effect of Aβ42 in setting of full pharmacological inhibition of γ-secretase suggests that Aβ42-mediated increases in APP-CTFs are mediated by both inhibition of γ-secretase as well as one or more additional mechanisms **(Figure 7D)**. Nevertheless, the greater relative accumulation of APP-CTFs in the absence (138%) **(Figure 5A)** versus the presence of the GSI (48%) **(Figure 7D)** is evidence that Aβ42-mediated γ-secretase inhibition plays a more incisive role.

APP-CTF levels are increased in Aβ42-treated synaptosomes derived from mouse brains

Since both the amyloidogenic processing of APP and the accumulation of Aβ occur at the synapse (*54, 55*), we reasoned that synaptosomes are potentially a cellular locus where elevated levels of Aβ could be acting on γ-secretase. Therefore, we tested γ-secretase-mediated processing of APP at the synapse and investigated whether Aβ42 inhibits γ-secretase at this particular locus **(Figure 8A)**. To this end, we prepared synaptosomes from wild type mouse brains, treated these fractions with 2.5 μM Aβ42 or vehicle, and then measured APP-FL and APP-CTF levels by western blotting. An increased APP-CTF/FL ratio in Aβ42 treated samples, compared to vehicle control, provided evidence of γ-secretase inhibition. We conclude that Aβ42 can impact endogenous processing of APP in synaptosomes, a biologically and pathophysiologically relevant structure.

DISCUSSION

Compelling evidence supports that Aβ peptides trigger molecular and cellular cascades that result in neurodegeneration (*56, 57*). Here, we discovered and thoroughly characterized a previously unreported role for Aβ: inhibition of γ-secretase complexes. The recognition that Aβ peptides, despite lower affinities, can compete with APP-CTFs for binding to γ-secretase, when present at relatively high concentrations (*30*), led us to propose a mechanism that connects increases in the Aβ42 peptide with inhibition of γ-secretases. We note that two different mechanisms involving γ-secretases are known to cause neurodegeneration: γ-secretase dysfunction in autosomal dominant FAD (*1*) and γ-secretase inhibition, leading to age-dependent neurodegenerative phenotypes in mice (*8-11*). The mechanisms underlying the detrimental effects of dysfunction and inhibition are poorly understood, though it is clear that the former implicates Aβ metabolism, while the second is independent of APP (*8*). In addition,

pharmacological inhibition of γ-secretase activity has been linked to cognitive worsening in AD affected individuals (*7*).

To explore the possible links between γ-secretase dysfunction (*1*) and γ-secretase inhibition (*8-11*) we analyzed γ-secretase endopeptidase activity in well-controlled cell-free assays, using purified protease and substrate. The data demonstrated that human Aβ42 inhibited the processing of APP_{C99} by all members of the human γ-secretase family. Notably, despite the high homology between human and murine Aβ sequences, murine Aβ1-42 peptide failed to inhibit the proteolysis of APP_{C99}, implying that structural determinants in the N-terminal domain of Aβ are involved in the inhibitory mechanism. Consistent with this view, N-terminally truncated Aβ peptides (Aβ11-42 and p3 17-42) demonstrated reduced or no inhibitory properties, compared to human Aβ42. Of note, the p3 peptide lacks the 16 amino acid long, hydrophilic and disordered N-terminal domain present in Aβ peptides, but does contain the two aggregation prone regions (16–21 and 29-42) required for the assembly of oligomers (*58, 59*) and fibrils (*60-62*). Despite p3 peptide's aggregation prone behavior (*22*) and accumulation in AD brain (*60, 63-65*), whether this peptide is responsible for toxicity is not well defined (*37*).

Our analyses in cell-free systems revealed that the C-terminus of Aβ also modulates its intrinsic inhibitory properties, with shorter Aβ1-x species (x= 37, 38, 40) either not acting as inhibitors or inhibiting the protease to a lesser degree than human Aβ42. The reported lower affinities of shorter Aβ peptides towards γ-secretase may, at least partially, explain their decreased inhibitory potencies (*30*). Further investigations on cultures of neurons and neuron-like cells showed that extracellularly applied human Aβ42 resulted in the accumulation of unprocessed γ-secretase substrates. Given that the accumulation of the substrates may stem from multiple cellular pathways, such as sheddase activation or protein degradation impairments, we quantified Aβ42-driven inhibition of γ-secretase using a live cell FRET-based imaging assay that is independent of the aforementioned alternative cellular processes, and hence specifically and selectively reports on the substrate proteolysis by endogenous γ-secretases. These analyses demonstrated a significant reduction in the global γ-secretase activity in neurons treated with human Aβ42, but not with p3.

In contrast to findings in cell-free assays, γ-secretase inhibition in cells was only observed for human Aβ42. Other Aβ and p3 peptides did not trigger the accumulation of unprocessed APP-CTFs.

Reports showing that Aβ conformation affects both cellular internalization and neurotoxicity (*66*) motivated us to test the possibility that Aβ42, unlike other Aβ peptides, acquires specific conformations that promote endocytosis and/or inhibit intracellular degradation. Earlier reports of the selective uptake of Aβ42, relative to Aβ40 (*46, 67-69*), facilitating concentration of Aβ42 in spatially restricted endosomal compartments, would support this postulation. Our data showing marked increases in the intracellular levels of Aβ42, but not Aβ40 or Aβ43, in cells add to the evidence for peptide-specific differences, but whether they are due to changes in cellular uptake, metabolism or both that lead to higher Aβ42 concentrations and product-feedback inhibition requires further study.

Evidence that Aβ42 exerts a general inhibition of γ-secretase activity is provided by data showing that this peptide also reduced processing of non-APP γ-secretase substrates, including NOTCH, neurexin, pan-cadherin and p75. The inhibitory curves revealed stronger inhibition of NOTCH than APP_{C99} cleavage, which may arise from the lower stability of γ-secretase interactions with NOTCH, relative to APP_{C99} (*30*). Considering the poor sequence homology between distinct γ-secretase substrates and the general Aβ-mediated inhibitory effect, we reason that the inhibitory action of Aβ42 likely involves its interaction with the protease, rather than with the substrate.

Having observed a general impact of Aβ42 on γ-secretase activity, we investigated the effects of Aβ42 on γ-secretase-mediated signaling. Specifically, our analyses demonstrated that treatment of BFCNs (or PC12 cells) with human Aβ42, but not with p3, compromised the processing of p75, increased p75-CTF levels and, in the absence of TrkA, triggered apoptotic cell death. These observations recapitulated reported findings showing that GSI treatment of BFCNs triggers p75-driven cell-death under similar conditions (*41*). Of note, these studies also showed that apoptosis in BFCNs subjected to GSI and TrkA signaling inhibitor treatments was rescued in p75 KO BFCNs, demonstrating that cell death is p75-dependent (*41*). Our findings showing that Aβ42 treatment mimics GSI-driven p75-dependent apoptosis in BFCNs support the inhibitory role of Aβ42 and links it to dysregulation of downstream signaling cascades. We note a prior study that showed that injection of Aβ42 into the hippocampus of adult mice resulted in the degeneration of choline acetyltransferase (ChAT)-positive forebrain neurons in wild type but not p75-NTR-deficient mice, a report that noted a correlation between

Aβ42-driven neuronal death and accumulation of p75-CTFs (*70, 71*). Our findings provide mechanistic bases for these observations.

Endocytic uptake of extracellular Aβ, the extracellular concentration of which is estimated to be at pM to low nM range in the brain, was shown to concentrate Aβ42 to μM levels in the endolysosomal compartments (*46, 48*). Within these compartments, the presence of peptides at high concentration and at low pH would serve to facilitate Aβ aggregation and toxicity. We speculate that this mechanism could in addition promote the inhibition of γ-secretases. Given the reported role for APP_{C99} in inducing dysregulation of the endolysosomal network, the potential Aβ42-mediated inhibition of γ-secretase processing of APP-CTFs could drive dysregulation of endolysosomal function leading to changes in synaptic, axonal signaling and degradative functions (*72-78*). Equally intriguing is the possibility that the inhibition of other γ-secretase substrates by Aβ42 could contribute to neurodegeneration, as reported previously for the genetic inactivation of these enzymes (*8-11*).

The Aβ-mediated inhibition of γ-secretase may also help to explain the intriguing accumulation of APP-CTFs in the heterozygous FAD brain (*79*). In this regard, the direct quantification of γ-secretase activity in detergent resistant fractions prepared from post-mortem brain samples of healthy controls and FAD-linked mutation carriers revealed similar overall γ-secretase activity levels, indicating that the normal (PSEN1 and PSEN2) γ-secretase complexes rescue any potential mutation-driven deficits in the processing of APP (*80*). Yet APP-CTFs have been reported to accumulate in the FAD brain (*79, 81*). The inhibition of γ-secretase by Aβ42 could resolve the apparent conflict. Our data could also reconcile two at first glance exclusive hypothesis on the effects of FAD mutations in *PSEN1* on the development of AD (*28, 82*). Specifically, the mutation-driven dysfunction on γ-secretase (*80*), leading to enhanced generation of Aβ42, may result in γ-secretase loss-of-function phenotypes that stem from the described here inhibitory effects.

Collectively, our data raise the intriguing possibility that local elevations in Aβ42 in the AD brain, and in particular in the endolysosomal compartment, facilitate the establishment of an Aβ-driven inhibitory mechanism that contributes to neurotoxicity by impairing critical γ-secretase signaling functions **(Figure 8B)**. Finally, by mechanistically connecting elevated Aβ42 levels with accumulation of multiple γ-secretase substrates, our observations integrate two pathways leading to neurodegeneration

and offer a novel conceptual framework for investigations of the molecular and cellular bases of AD pathogenesis.

MATERIALS AND METHODS

Chemicals, peptides and antibodies

Aβ peptides were purchased from rPeptide, resuspended in DMSO at 500 μM, aliquoted into single use 10 μl aliquots and stored at -80ºC. Γ-secretase inhibitors (Inhibitor X (InhX, L-685,458), DAPT and compound E (CE)) were purchased from Bioconnect, Sigma Aldrich and Millipore, respectively. TrkA inhibitor K252α, cycloheximide and Bafilomycin A1 were purchased from Sigma Aldrich. The following antibodies were used: mouse anti-FLAG M2 (Sigma Aldrich, F3165), rabbit anti-ADAM10 antibody (EPR5622, Abcam, ab124695), rabbit anti-APP (gift from Prof. Wim Annaert (B63)), rabbit anti-APP (Y188, Abcam, ab32136), mouse anti-APP (22C11, Thermo Fisher Scientific, 14-9749-82), rabbit anti-BACE1 (EPR19523, Abcam, ab183612), rabbit anti-pan-cadherin (Thermo Fisher Scientific, 71-7100), anti-p75 NTR (Millipore, 07-476), anti-Aβ (clone 4G8, Biolegend), anti-choline acetyltransferase (Millipore, AB144P), anti-cleaved caspase-3 (Cell Signaling, 9661S), HRP-conjugated goat anti-rabbit (BioRad), Alexa Fluor 790-conjugated goat anti-mouse (Thermo Fisher Scientific), Cy3-conjugated donkey anti-rabbit (Jackson ImmunoResearch Laboratories), Alexa Fluor Plus 488-conjugated donkey anti-mouse (Thermo Fisher Scientific), biotinylated rabbit anti-goat (Jackson ImmunoResearch Laboratories) and Cy2-conjugated streptavidin (Jackson Immunoresearch Laboratories).

AAV production

Preparation of the AAV-hSyn1-C99 Y-T biosensor was performed as described previously (*45*). Briefly, the cDNA of C99 Y-T probe was subcloned into a pAAV2/8 vector containing human synapsin 1 promoter and WPRE sequences (*83*). The packaging into viruses was performed at University of Pennsylvania Gene Therapy Program vector core (Philadelphia, PA). The virus titer was 4.95E+13 GC/ml.

Γ-secretase and γ-secretase substrate expression and purification

High Five insect cells were transduced with baculoviruses carrying cDNA encoding all γ-secretase subunits (wild type PSEN1 or PSEN2, NCSTN, APH1A or APH1B, PEN2) and 72 hours later the cells were collected for protein purification, as described before (*30*).

Recombinant γ-secretase substrates were expressed and purified using mammalian cell expression system or baculovirus-mediated expression system in High Five insect cells as before (*30, 41, 84*). COS cells were transfected with pSG5 plasmid encoding NOTCH1- or P75-based γ-secretase substrate, tagged at the C-terminus with 3xFLAG. High Five insect cells were transduced with baculoviruses carrying cDNA encoding APP_{C99}, ERBB4ΔECT and neurexinΔECT-tagged with 3xFLAG-prescission protease (PPS) cleavage site-GFP tandem at the C-terminus. The purity of the protein was analyzed by SDS-PAGE and Coomassie staining (InstantBlue Protein Stain, Expedeon).

Preparation of detergent resistant membranes

CHAPSO detergent resistant membranes (DRMs) were prepared from High Five insect cells overexpressing wild type γ-secretase complexes containing NCSTN, APH1B, PSEN1 and PEN2 subunits, as reported before (*30*).

Cell-free γ-secretase activity assays

Purified γ-secretases (~25 nM) were mixed with respective, purified 3xFLAG-tagged γ-secretase substrates (0.4 or 1.2 μM) in 150 mM NaCl, 25 mM PIPES, 0.25% CHAPSO, 0.03% DDM, 0.1% phosphatidylcholine buffer and the reactions were incubated for 40 minutes at 37°C. Non-incubated reactions or reactions supplemented with 10 μM InhX served as negative controls. In the experiments testing for the reversibility of the inhibition, γ-secretases were first immobilized on sepharose beads covalently coupled to anti-γ-secretase nanobody. Following the first reaction containing Aβ or GSI, the beads were washed 3x for a total duration of 30 minutes with 150 mM NaCl, 25 mM PIPES, 0.25% CHAPSO buffer and a fresh substrate was added. For γ-secretase activity assays in membrane-like conditions (25 μl total reaction volume), 6.25 μl DRMs, re-suspended in 20 mM PIPES, 250 mM sucrose, 1 M EGTA, pH7 at the concentration of 1 μg/μl, were mixed with 6.25 μl APP_{C99}-

3xFLAG or Aβ1-42 substrate in 150 mM NaCl, 25 mM PIPES, 0.03% DDM, 2.5 µl 10xMBS and H_2O supplemented with DDM and CHAPSO, to achieve final concentration of the detergents 0.03% and 0.1%, respectively, and final concentration of the substrates 1.5 µM and 10 µM, respectively. The reaction mixes were incubated for 40 minutes at 37ºC. Reactions supplemented with 10 µM InhX served as negative controls.

Analysis of ICD generation in cell-free γ-secretase activity assays

De novo ICD generation was determined by western blotting. Briefly, the reaction mixtures were subjected to methanol:chloroform (1:2 v/v) extraction to remove the excess of unprocessed substrates, and the upper fractions (containing mainly the generated ICDs) subjected to SDS-PAGE. Otherwise, the high levels of substrate could preclude quantitative analysis of ICDs **(Supplementary figure 1).**

ICD-3xFLAG were detected by western blotting with anti-FLAG, followed by anti-mouse Alexa Fluor 790 conjugated antibodies. Fluorescent signals were developed using Typhoon (GE Healthcare). The intensity of the bands was quantified by densitometry using ImageQuant software.

Alternatively, MALDI-TOF MS was applied to determine the relative *de novo* ICD-3xFLAG levels generated in cell-free conditions, as reported before (*30*). The samples were spiked with Aβ1-28 as an internal standard. The mass spectra were acquired on a RapiFleX TOF mass spectrometer (Bruker Daltonics) equipped with a 10 kHz Smartbeam™ laser using the AutoXecute function of the FlexControl 4.2 acquisition software.

Analysis of γ-secretase substrate proteolysis in cultured cells

SH-SY5Y, PC12 and PC12nnr5 (*52*) cell lines were cultured in Dulbecco's Modified Eagle Medium (DMEM)/F-12 (Thermo Fisher Scientific) supplemented with 10% fetal bovine serum (FBS) (Gibco) at 37ºC, 5% CO_2. ReNCell VM cells were cultured in Corning® Matrigel® hESC-Qualified Matrix, LDEV-free-coated flasks in DMEM/F-12 medium supplemented with B27 (Thermo Fisher Scientific), 2 µg/ml heparin (Stem Cell Technologies), 20 ng/ml EGF-1 (Cell Guidance) and 25 ng/ml FGF (Cell Guidance). Human iPSC line was derived from a cognitively unaffected male individual,

previously established and characterized (CVB) (RRID: CVCL_1N86, GM25430) (*85*). The two neuronal progenitor cell (NPC) lines – CV4a (derived from CVB iPSC line that carries a wild type APP, herein termed as WT) and APPSwe (homozygous for APP Swedish mutations that were genome-edited from CVB parental iPSC line) were characterized and reported (*86, 87*). NPCs were plated on 20 µg/ml poly-L-ornithine (Sigma Aldrich) and 5 µg/ml laminin (Thermo Fisher Scientific)-coated plates in NPC media: DMEM/F12/Glutamax supplemented with N2, B27, penicillin and streptomycin (Thermo Fisher Scientific) and 20 ng/ml FGF-2 (Millipore). For neuronal differentiation, confluent NPCs were cultured in NPC media without FGF-2 for three weeks. All cells were maintained in a humidified incubator at 37ºC, 5% CO_2, and regularly tested for mycoplasma infection.

For the cellular assays, cells were plated into 6-well plates at the density of 300000 cells per well and 24h after plating treated with Aβ or p3 peptides diluted in OPTIMEM (Thermo Fisher Scientific) supplemented with 5% FBS (Gibco). In the experiments set to analyze sAPP in the conditioned medium, FBS was replaced with 1% knock-out serum replacement (KOSR) (Thermo Fisher Scientific) due to the interference of the antibodies present in the serum with western blotting. After 8h, the medium was refreshed, using peptide supplemented media, and the cultures were incubated at 37°C for 16h. Cell lysates were prepared in radioimmunoprecipitation (RIPA) buffer (25 mM Tris, 150 mM NaCl, 1% Nonidet P-40, 0.5% sodium deoxycholate, 0.1% SDS, pH 7.4) supplemented with protease inhibitors. Equal amounts of protein or conditioned medium were subjected to SDS-PAGE on 4-12% Bis-Tris gels in MES or MOPS buffer or 4-16 % Tris-Tricine gels (*88*) and western blot analysis. Chemiluminescent signals were developed using Fujifilm LAS-3000 Imager or ChemiDoc XRS+ imaging apparatus (BioRad). The optical density of the bands was quantified using ImageQuant or Image J software.

Cytotoxicity assays

Cytotoxicity was assessed using LDH-Glo Cytotoxicity Assay (Promega), which is a bioluminescent plate-based assay for quantifying LDH release into the culture medium upon plasma membrane damage. The assay was performed following the manufacturer recommendation. Briefly, culture medium was collected upon respective treatment and diluted 1 in 100 in LDH storage buffer

(200mM Tris-HCl (pH 7.3), 10% glycerol, 1% BSA). Medium from cells treated for 15 min with 2% Triton X-100 was used as a maximum LDH release control. 12.5 µl of diluted medium was mixed with 12.5 µl LDH detection enzyme mix supplemented with reductase substrate in 384-well plate. The reactions were incubated for 1h and luminescence read using Promega GloMax Discoverer.

Cytotoxicity was also assessed using CellTiter-Glo® 2.0 Assay (Promega), which is a homogeneous method used to determine the number of viable cells based on quantitation of the ATP, an indicator of metabolically active cells. Briefly, cells were plate in 96-well plate in 100 µl medium, treated following the treatment regime, mixed with CellTiter-Glo reagent and luminescence was read using Promega GloMax Discoverer.

Isolation of biologically derived human Aβ and cellular assay for γ-secretase-mediated proteolysis

The conditioned media from the WT (WT-CM) and APPSwe (SWE-CM) human neurons were used as a biological source of Aβ. Following three weeks of differentiation, neurons cultured on 10 cm diameter dishes were incubated in NPC media without FGF-2 for five days. After five days, conditioned media were collected in a sterile atmosphere. Immunodepletion of Aβ from APPSwe medium was done following a modified protocol (*89*). Briefly, 5 ml of SWE-CM were incubated with 3D6 antibody (1 µg/ml), 15 µl protein A and 15 µl protein G resin for 3h at 4°C with gentle shaking on a nutator (*90*). The supernatant was collected after centrifuging at 3500×g and used as immunodepleted media (delSWE-CM) for cell culture experiments. To test for the APP-CTF accumulation in the presence of different conditioned media, PC12 cells, cultured on 6-well plates, were treated with WT-CM, SWE-CM or delSWE-CM for 24h along with regular feeding media (control). Following incubation, cells were harvested and processed to detect APP-FL and APP-CTF.

Spectral FRET analysis of γ-secretase activity in living neurons

Primary neuronal cultures were obtained from cerebral cortex of mouse embryos at gestation day 14–16 (Charles River Laboratories). The neurons were dissociated using Papain Dissociation System (Worthington Biochemical Corporation, Lakewood, NJ) and maintained for 13-15 days *in vitro* (DIV) in neurobasal medium containing 2% B27, 1% GlutaMAX Supplement and 1%

penicillin/streptomycin (Thermo Fisher Scientific). A laser at 405 nm wavelength was used to excite TurquoiseGL in the C99 Y-T biosensor (*45*). The emitted fluorescence from the donors (TurquoiseGL) and the acceptors (YPet) was detected at 470±10nm and 530±10nm, respectively, by the TruSpectral detectors on an Olympus FV3000RS confocal microscope equipped with CO_2/heating units. x10/0.25 objective was used for the imaging. Average pixel fluorescence intensity for the cell body after subtraction of the background fluorescence was measured using Image J. The emission intensity of YPet over that of TurquoiseGL (Y/T) ratio was used as a readout of the FRET efficiency, which reflects the relative proximity between the donor and the acceptor. Pseudo-colored images were generated in MATLAB (MathWorks, Natick, MA). The neuronal preparation procedure followed the NIH guidelines for the use of animals in experiments and was approved by the Massachusetts General Hospital Animal Care and Use Committee (2003N000243).

Primary cultures of basal forebrain cholinergic neurons

Animals of CD1 genetic background were housed in an animal care facility with a 12-hour dark/light cycle and had free access to food and water. All experiments were performed according to the animal care guidelines of the European Community Council (86/609/EEC) and to Spanish regulations (RD1201 / 2005), following protocols approved by the ethics committees of the Consejo Superior Investigaciones Científicas (CSIC). Septal areas were dissected from CD1 E17-18 embryos in chilled Hanks' balanced salt solution (HBSS, 137 mM NaCl, 5.4 mM KCl, 0.17 mM Na_2HPO_4, 0.22 mM KH_2PO_4, 9.9 mM HEPES, 8.3 mM glucose and 11 mM sucrose). The septa were pooled and digested with 1 ml of 0.25% trypsin (GE Healthcare) and 0.5 ml of 100 kU DNase I (GE healthcare) for 10 minutes at 37ºC. The tissue was further dissociated by aspiration with progressively narrower tips in neurobasal medium (Thermo Fisher Scientific) supplemented with 4% bovine serum albumin (BSA), 2% B27 (Thermo Fisher Scientific), 1% L-glutamine (Thermo Fisher Scientific) and 0.5% penicillin/streptomycin (GE Healthcare) (NB/B27). After tissue dissociation, equal volume of 4% BSA was added and samples centrifuged at 300xg for 5 minutes at 4ºC. The supernatant was discarded and the cell pellet resuspended in 5 ml of 0.2% BSA. The suspension was filtered through 40 µm nylon filter (Sysmex), cells counted in Neubauer chamber, centrifuged again and resuspended in NB/B27. Cells

were seeded in 24-well plates ($2x10^5$ cells/well) containing 12 mm diameter pre-coated coverslips (VWR) for immunocytochemical analysis or in pre-coated p-100 plates for western blotting. The surfaces were coated with 50 µg/ml poly-D-lysine (Sigma Aldrich) overnight at 4°C and 5 µg/ml laminin (Sigma Aldrich) for 2h at 37°C. The next day, half of the medium was exchanged and the concentration of B27 reduced to 0.2%. The medium was supplemented with 2 µM of the antimitotic agent (1-β-D-Arabinofuranosylcytosine (Sigma Aldrich)) and 100 ng/ml NGF (Alomone labs). Neurons were cultured until DIV11. The respective treatments were applied at DIV8 and the culture continued for 72h until DIV11.

Immunocytochemical analysis of the cell death rate

For immunocytochemistry (ICC) cells were fixed in 2% paraformaldehyde and permeabilized with 0.1% Triton X-100. After that they were incubated with 0.5% SDS for 5 minutes for antigen retrieval. Non-specific binding of antibodies was blocked using 2% BSA, 0.1% Triton X-100 in 0.1 M phosphate buffer (PB). The cells were incubated overnight with anti-choline acetyltransferase (Millipore) (only for BFCN) and anti-cleaved caspase-3 (Cell Signaling) antibodies at 4°C. The next day the samples were incubated with corresponding secondary antibodies: Cy3-conjugated donkey anti-rabbit, biotinylated rabbit anti-goat, and Cy2-conjugated streptavidin (all purchased from Jackson Immunoresearch Laboratories). Nuclei were stained with DAPI and samples mounted on glass slides. For quantitative analysis, for BFCNs total number of choline acetyltransferase positive neurons and the number of double positive neurons for choline acetyltransferase and cleaved caspase-3 was determined, while for PC12 a fraction of cleaved caspase 3 positive cells among all cells (determined by DAPI staining) was determined.

Immunocytochemical analysis of Aβ internalization

PC12 cells were plated on glass coverslips and treated for 24h with respective Aβ peptides at 1 µM. The cells were fixed with 4% paraformaldehyde, and permeabilized with 0.5% Triton X-100 in TBST (0.2% Tween 20 in TBS). Blocking was performed by 1h incubation in solution containing 1% bovine serum albumin, 0.1% gelatin, 300 mM glycine and 4% normal donkey serum in TBST. Primary

antibodies were diluted in the blocking solution and incubated overnight. This was followed by incubation with respective Alexa Fluor Plus 488 conjugated secondary antibody and Alexa Fluor Plus 555 conjugated phalloidin. The samples were then incubated with nuclear stain DAPI for 5 min and mounted using Prolong glass. Images were acquired at 63x magnification using Zeiss LSM 900 confocal microscope at VIB Bioimaging Core.

Measurement of APP-CTF levels in peptide-treated synaptosomes from mouse cortical tissue

The cortical tissues from two-months old wild-type mice (N=3) were collected and stored at -80°C. Synaptosomes from the cortices were isolated following published protocol using a discontinuous Percoll gradient (Sigma Aldrich, USA) (*91, 92*) with some modifications. All the steps were performed on ice or at 4°C unless mentioned otherwise. Briefly, 60-70 mg of tissue was homogenized using a handhold Dounce homogenizer in 5 volumes of homogenization buffer (HB: 0.32 M sucrose, 5 mM magnesium chloride, 5 mM Tris-Cl, pH 7.4 and EDTA-free protease inhibitor cocktail). After centrifuging at 1000xg for 10 minutes, post-nuclear supernatant (PNS) was collected. The PNS was further centrifuged at 10800xg for 10 minutes to isolate the pellet fractions (P2, crude synaptosome). The P2 fraction was resuspended in HB and loaded on top of a three-step (3%, 10% and 23%) Percoll gradient, and centrifuged at 14500xg for 12 minutes at 4°C in a Fiberlite F21-8 x 50y Fixed-Angle Rotor (Thermo Fisher, USA). The synaptosome-rich interface between 10% and 23% Percoll layers was collected and resuspended in 30 volumes of HB. The diluted material was centrifuged at 18500xg for 30 minutes at 4°C, and the synaptosome-enriched pellet was resuspended in HB supplemented with 10 mM glucose. 10-15 µg of synaptosome was incubated with Aβ42 peptide at 2.5 µM final concentration at 37°C for 18h. DMSO was used as a vehicle control. One synaptosomal sample was treated with 200 nM of Compound E. Following incubation, samples were resolved on SDS-PAGE and western blotting was performed using anti-APP Y188 and anti-GAPDH antibodies. All densitometric analyses were performed using NIH ImageJ software. The animal experiments were approved by the Institutional Animal Care and Use Committee of the University of California San Diego.

Statistics

Statistical analysis was performed using Excel, GraphPad Prism, R 4.2.2. and R Studio software. The following R packages were used for the analysis: readxl, ggplot2, plyr, dplyr, DescTools, gridExtra and reshape2 (*93-95*). $P<0.05$ was considered as a predetermined threshold for statistical significance. One-way or two-way ANOVA, or Kruskal-Wallis test followed by Dunnett's, Tukey's or Dunn multiple comparison test or unpaired Student's t-test were used, as described in the legends.

ACKNOWLEDGEMENTS

This work was supported by the Cure Alzheimer's Fund (WCM-LCG), the Research Foundation Flanders (FWO, Research project G0B2519N) (LCG), the DH Chen Foundation (WCM), NIH AG015379 (OB), NIH AG044486 (OB), NIH R01AG055523 (WCM) and Bundesministerium für Bildung und Forschung (BMBF) grant M^2OGA within the Partnership for Innovation in Health Industry, M^2Aind (CH). MV acknowledges the Spanish Ministry of Science and Innovation (grant PID2021-127600NB-I00). We would like to thank VIB Bioimaging Core for support with confocal imaging and Dr Laetitia Miguel for support in the culture of ReNcell VM cells. We thank all the Mobley and Chávez-Gutiérrez lab members for fruitful discussions.

REFERENCES

1. L. Chávez-Gutiérrez, M. Szaruga, Mechanisms of neurodegeneration - Insights from familial Alzheimer's disease. *Semin Cell Dev Biol* **105**, 75-85 (2020).
2. D. J. Selkoe, J. Hardy, The amyloid hypothesis of Alzheimer's disease at 25 years. *EMBO Mol Med* **8**, 595-608 (2016).
3. A. Haapasalo, D. M. Kovacs, The many substrates of presenilin/γ-secretase. *J Alzheimers Dis* **25**, 3-28 (2011).
4. G. Güner, S. F. Lichtenthaler, The substrate repertoire of γ-secretase/presenilin. *Semin Cell Dev Biol* **105**, 27-42 (2020).
5. N. Jurisch-Yaksi, R. Sannerud, W. Annaert, A fast growing spectrum of biological functions of γ-secretase in development and disease. *Biochim Biophys Acta* **1828**, 2815-2827 (2013).
6. C. M. Carroll, Y.-M. Li, Physiological and pathological roles of the γ-secretase complex. *Brain Research Bulletin* **126**, 199-206 (2016).

7. R. S. Doody *et al.*, A phase 3 trial of semagacestat for treatment of Alzheimer's disease. *N Engl J Med* **369**, 341-350 (2013).

8. H. Acx *et al.*, Inactivation of γ-secretases leads to accumulation of substrates and non-Alzheimer neurodegeneration. *EMBO Mol Med* **9**, 1088-1099 (2017).

9. M. Wines-Samuelson *et al.*, Characterization of age-dependent and progressive cortical neuronal degeneration in presenilin conditional mutant mice. *PLoS One* **5**, e10195 (2010).

10. K. Tabuchi, G. Chen, T. C. Südhof, J. Shen, Conditional forebrain inactivation of nicastrin causes progressive memory impairment and age-related neurodegeneration. *J Neurosci* **29**, 7290-7301 (2009).

11. C. A. Saura *et al.*, Loss of presenilin function causes impairments of memory and synaptic plasticity followed by age-dependent neurodegeneration. *Neuron* **42**, 23-36 (2004).

12. H. R. Bi *et al.*, Neuron-specific deletion of presenilin enhancer2 causes progressive astrogliosis and age-related neurodegeneration in the cortex independent of the Notch signaling. *CNS Neurosci Ther* **27**, 174-185 (2021).

13. M. Maesako, M. C. Q. Houser, Y. Turchyna, M. S. Wolfe, O. Berezovska, Presenilin/γ-Secretase Activity Is Located in Acidic Compartments of Live Neurons. *J Neurosci* **42**, 145-154 (2022).

14. R. Vassar *et al.*, Beta-secretase cleavage of Alzheimer's amyloid precursor protein by the transmembrane aspartic protease BACE. *Science* **286**, 735-741 (1999).

15. M. Takami *et al.*, gamma-Secretase: successive tripeptide and tetrapeptide release from the transmembrane domain of beta-carboxyl terminal fragment. *J Neurosci* **29**, 13042-13052 (2009).

16. D. M. Bolduc, D. R. Montagna, M. C. Seghers, M. S. Wolfe, D. J. Selkoe, The amyloid-beta forming tripeptide cleavage mechanism of γ-secretase. *Elife* **5**, (2016).

17. L. Chávez-Gutiérrez *et al.*, The mechanism of γ-Secretase dysfunction in familial Alzheimer disease. *Embo j* **31**, 2261-2274 (2012).

18. Y. Qi-Takahara *et al.*, Longer forms of amyloid beta protein: implications for the mechanism of intramembrane cleavage by gamma-secretase. *J Neurosci* **25**, 436-445 (2005).

19. S. Funamoto *et al.*, Truncated carboxyl-terminal fragments of beta-amyloid precursor protein are processed to amyloid beta-proteins 40 and 42. *Biochemistry* **43**, 13532-13540 (2004).

20. N. Kakuda *et al.*, Distinct deposition of amyloid-β species in brains with Alzheimer's disease pathology visualized with MALDI imaging mass spectrometry. *Acta Neuropathol Commun* **5**, 73 (2017).

21. L. Fu *et al.*, Comparison of neurotoxicity of different aggregated forms of Aβ40, Aβ42 and Aβ43 in cell cultures. *J Pept Sci* **23**, 245-251 (2017).

22. A. J. Kuhn, J. Raskatov, Is the p3 Peptide (Aβ17-40, Aβ17-42) Relevant to the Pathology of Alzheimer's Disease?1. *J Alzheimers Dis* **74**, 43-53 (2020).

23. S. F. Lichtenthaler, α-secretase in Alzheimer's disease: molecular identity, regulation and therapeutic potential. *J Neurochem* **116**, 10-21 (2011).

24. M. D. Tambini, K. A. Norris, L. D'Adamio, Opposite changes in APP processing and human Aβ levels in rats carrying either a protective or a pathogenic APP mutation. *Elife* **9**, (2020).

25. M. Mullan *et al.*, A pathogenic mutation for probable Alzheimer's disease in the APP gene at the N-terminus of beta-amyloid. *Nature genetics* **1**, 345-347 (1992).

26. M. Pagnon de la Vega *et al.*, The Uppsala APP deletion causes early onset autosomal dominant Alzheimer's disease by altering APP processing and increasing amyloid β fibril formation. *Science translational medicine* **13**, (2021).

27. I. E. Jansen *et al.*, Genome-wide meta-analysis identifies new loci and functional pathways influencing Alzheimer's disease risk. *Nat Genet* **51**, 404-413 (2019).

28. S. Veugelen, T. Saito, T. C. Saido, L. Chávez-Gutiérrez, B. De Strooper, Familial Alzheimer's Disease Mutations in Presenilin Generate Amyloidogenic Aβ Peptide Seeds. *Neuron* **90**, 410-416 (2016).

29. M. A. Fernandez, J. A. Klutkowski, T. Freret, M. S. Wolfe, Alzheimer presenilin-1 mutations dramatically reduce trimming of long amyloid β-peptides (Aβ) by γ-secretase to increase 42-to-40-residue Aβ. *J Biol Chem* **289**, 31043-31052 (2014).

30. M. Szaruga *et al.*, Alzheimer's-Causing Mutations Shift Aβ Length by Destabilizing γ-Secretase-Aβn Interactions. *Cell* **170**, 443-456.e414 (2017).

31. S. Devkota, T. D. Williams, M. S. Wolfe, Familial Alzheimer's disease mutations in amyloid protein precursor alter proteolysis by γ-secretase to increase amyloid β-peptides of >45 residues. *J Biol Chem*, 100281 (2021).

32. B. Kretner *et al.*, Generation and deposition of Aβ43 by the virtually inactive presenilin-1 L435F mutant contradicts the presenilin loss-of-function hypothesis of Alzheimer's disease. **8**, 458-465 (2016).

33. D. Petit *et al.*, Aβ profiles generated by Alzheimer's disease causing PSEN1 variants determine the pathogenicity of the mutation and predict age at disease onset. *Molecular Psychiatry*, (2022).

34. K. G. Mawuenyega *et al.*, Decreased clearance of CNS beta-amyloid in Alzheimer's disease. *Science (New York, N.Y.)* **330**, 1774 (2010).

35. L. Liu *et al.*, Identification of the Aβ37/42 peptide ratio in CSF as an improved Aβ biomarker for Alzheimer's disease. *Alzheimers Dement*, (2022).

36. G. Brinkmalm *et al.*, Identification of neurotoxic cross-linked amyloid-β dimers in the Alzheimer's brain. *Brain* **142**, 1441-1457 (2019).

37. D. M. Walsh *et al.*, Naturally secreted oligomers of amyloid beta protein potently inhibit hippocampal long-term potentiation in vivo. *Nature* **416**, 535-539 (2002).

38. W. Hong *et al.*, Diffusible, highly bioactive oligomers represent a critical minority of soluble Aβ in Alzheimer's disease brain. *Acta Neuropathol* **136**, 19-40 (2018).

39. Z. Wang *et al.*, Human Brain-Derived Aβ Oligomers Bind to Synapses and Disrupt Synaptic Activity in a Manner That Requires APP. *J Neurosci* **37**, 11947-11966 (2017).

40. I. Lauritzen, R. Pardossi-Piquard, A. Bourgeois, A. Bécot, F. Checler, Does Intraneuronal Accumulation of Carboxyl-terminal Fragments of the Amyloid Precursor Protein Trigger Early Neurotoxicity in Alzheimer's Disease? *Curr Alzheimer Res* **16**, 453-457 (2019).

41. M. L. Franco *et al.*, TrkA-mediated endocytosis of p75-CTF prevents cholinergic neuron death upon γ-secretase inhibition. *Life Sci Alliance* **4**, (2021).

42. N. Matsumura *et al.*, gamma-Secretase associated with lipid rafts: multiple interactive pathways in the stepwise processing of beta-carboxyl-terminal fragment. *J Biol Chem* **289**, 5109-5121 (2014).

43. C. C. Shelton *et al.*, A miniaturized 1536-well format gamma-secretase assay. *Assay Drug Dev Technol* **7**, 461-470 (2009).

44. M. C. Houser *et al.*, A Novel NIR-FRET Biosensor for Reporting PS/γ-Secretase Activity in Live Cells. *Sensors (Basel)* **20**, (2020).

45. M. Maesako *et al.*, Visualization of PS/γ-Secretase Activity in Living Cells. *iScience* **23**, 101139 (2020).

46. X. Hu *et al.*, Amyloid seeds formed by cellular uptake, concentration, and aggregation of the amyloid-beta peptide. *Proc Natl Acad Sci U S A* **106**, 20324-20329 (2009).

47. Y. Su, P. T. Chang, Acidic pH promotes the formation of toxic fibrils from beta-amyloid peptide. *Brain Res* **893**, 287-291 (2001).

48. M. P. Schützmann *et al.*, Endo-lysosomal Aβ concentration and pH trigger formation of Aβ oligomers that potently induce Tau missorting. *Nat Commun* **12**, 4634 (2021).

49. K. Uemura *et al.*, Characterization of sequential N-cadherin cleavage by ADAM10 and PS1. *Neurosci Lett* **402**, 278-283 (2006).

50. L. W. Wong, Z. Wang, S. R. X. Ang, S. Sajikumar, Fading memories in aging and neurodegeneration: Is p75 neurotrophin receptor a culprit? *Ageing Res Rev* **75**, 101567 (2022).

51. J. N. Conroy, E. J. Coulson, High-affinity TrkA and p75 neurotrophin receptor complexes: a twisted affair. *J Biol Chem*, 101568 (2022).

52. D. M. Loeb *et al.*, The trk proto-oncogene rescues NGF responsiveness in mutant NGF-nonresponsive PC12 cell lines. *Cell* **66**, 961-966 (1991).

53. T. Schneider-Poetsch *et al.*, Inhibition of eukaryotic translation elongation by cycloheximide and lactimidomycin. *Nat Chem Biol* **6**, 209-217 (2010).

54. E. K. Pickett *et al.*, Non-Fibrillar Oligomeric Amyloid-β within Synapses. *J Alzheimers Dis* **53**, 787-800 (2016).

55. S. Schedin-Weiss, I. Caesar, B. Winblad, H. Blom, L. O. Tjernberg, Super-resolution microscopy reveals γ-secretase at both sides of the neuronal synapse. *Acta Neuropathol Commun* **4**, 29 (2016).

56. P. Scheltens *et al.*, Alzheimer's disease. *Lancet* **397**, 1577-1590 (2021).

57. D. S. Knopman *et al.*, Alzheimer disease. *Nat Rev Dis Primers* **7**, 33 (2021).

58. G. Festa *et al.*, Aggregation States of A. *Int J Mol Sci* **20**, (2019).

59. F. Dulin *et al.*, P3 peptide, a truncated form of A beta devoid of synaptotoxic effect, does not assemble into soluble oligomers. *FEBS Lett* **582**, 1865-1870 (2008).

60. L. S. Higgins, G. M. Murphy, L. S. Forno, R. Catalano, B. Cordell, P3 beta-amyloid peptide has a unique and potentially pathogenic immunohistochemical profile in Alzheimer's disease brain. *Am J Pathol* **149**, 585-596 (1996).

61. M. López de la Paz, L. Serrano, Sequence determinants of amyloid fibril formation. *Proc Natl Acad Sci U S A* **101**, 87-92 (2004).

62. A. J. Kuhn, B. S. Abrams, S. Knowlton, J. A. Raskatov, Alzheimer's Disease "Non-amyloidogenic" p3 Peptide Revisited: A Case for Amyloid-α. *ACS Chem Neurosci* **11**, 1539-1544 (2020).

63. T. C. Saido, W. Yamao-Harigaya, T. Iwatsubo, S. Kawashima, Amino- and carboxyl-terminal heterogeneity of beta-amyloid peptides deposited in human brain. *Neurosci Lett* **215**, 173-176 (1996).

64. M. Lalowski *et al.*, The "nonamyloidogenic" p3 fragment (amyloid beta17-42) is a major constituent of Down's syndrome cerebellar preamyloid. *J Biol Chem* **271**, 33623-33631 (1996).

65. E. Gowing *et al.*, Chemical characterization of A beta 17-42 peptide, a component of diffuse amyloid deposits of Alzheimer disease. *J Biol Chem* **269**, 10987-10990 (1994).

66. D. M. Vadukul *et al.*, Internalisation and toxicity of amyloid-β 1-42 are influenced by its conformation and assembly state rather than size. *FEBS Lett* **594**, 3490-3503 (2020).

67. E. Wesén, G. D. M. Jeffries, M. Matson Dzebo, E. K. Esbjörner, Endocytic uptake of monomeric amyloid-β peptides is clathrin- and dynamin-independent and results in selective accumulation of Aβ(1-42) compared to Aβ(1-40). *Sci Rep* **7**, 2021 (2017).

68. D. Ling, M. Magallanes, P. M. Salvaterra, Accumulation of amyloid-like Aβ1-42 in AEL (autophagy-endosomal-lysosomal) vesicles: potential implications for plaque biogenesis. *ASN Neuro* **6**, (2014).

69. B. A. Bahr *et al.*, Amyloid beta protein is internalized selectively by hippocampal field CA1 and causes neurons to accumulate amyloidogenic carboxyterminal fragments of the amyloid precursor protein. *J Comp Neurol* **397**, 139-147 (1998).

70. A. Sotthibundhu *et al.*, Beta-amyloid(1-42) induces neuronal death through the p75 neurotrophin receptor. *J Neurosci* **28**, 3941-3946 (2008).

71. E. J. Coulson *et al.*, p75 neurotrophin receptor mediates neuronal cell death by activating GIRK channels through phosphatidylinositol 4,5-bisphosphate. *J Neurosci* **28**, 315-324 (2008).

72. W. Xu *et al.*, Amyloid precursor protein-mediated endocytic pathway disruption induces axonal dysfunction and neurodegeneration. *J Clin Invest* **126**, 1815-1833 (2016).

73. A. M. Weissmiller *et al.*, A γ-secretase inhibitor, but not a γ-secretase modulator, induced defects in BDNF axonal trafficking and signaling: evidence for a role for APP. *PLoS One* **10**, e0118379 (2015).

74. M. Sawa *et al.*, Impact of increased APP gene dose in Down syndrome and the Dp16 mouse model. *Alzheimers Dement* **18**, 1203-1234 (2022).

75. A. Salehi *et al.*, Increased App expression in a mouse model of Down's syndrome disrupts NGF transport and causes cholinergic neuron degeneration. *Neuron* **51**, 29-42 (2006).

76. D. Kwart *et al.*, A Large Panel of Isogenic APP and PSEN1 Mutant Human iPSC Neurons Reveals Shared Endosomal Abnormalities Mediated by APP β-CTFs, Not Aβ. *Neuron* **104**, 1022 (2019).

77. Y. Jiang *et al.*, Lysosomal Dysfunction in Down Syndrome Is APP-Dependent and Mediated by APP-βCTF (C99). *J Neurosci* **39**, 5255-5268 (2019).

78. S. Kim *et al.*, Evidence that the rab5 effector APPL1 mediates APP-βCTF-induced dysfunction of endosomes in Down syndrome and Alzheimer's disease. *Mol Psychiatry* **21**, 707-716 (2016).

79. M. Pera *et al.*, Distinct patterns of APP processing in the CNS in autosomal-dominant and sporadic Alzheimer disease. *Acta Neuropathol* **125**, 201-213 (2013).

80. M. Szaruga *et al.*, Qualitative changes in human γ-secretase underlie familial Alzheimer's disease. *J Exp Med* **212**, 2003-2013 (2015).

81. P. Ferrer-Raventós *et al.*, Amyloid precursor protein. *Neuropathol Appl Neurobiol* **49**, e12879 (2023).

82. J. Shen, R. J. Kelleher, The presenilin hypothesis of Alzheimer's disease: evidence for a loss-of-function pathogenic mechanism. *Proc Natl Acad Sci U S A* **104**, 403-409 (2007).

83. M. Maesako *et al.*, Pathogenic PS1 phosphorylation at Ser367. *Elife* **6**, (2017).

84. L. Chavez-Gutierrez *et al.*, The mechanism of gamma-Secretase dysfunction in familial Alzheimer disease. *EMBO J* **31**, 2261-2274 (2012).

85. A. Gore *et al.*, Somatic coding mutations in human induced pluripotent stem cells. *Nature* **471**, 63-67 (2011).

86. J. E. Young *et al.*, Elucidating molecular phenotypes caused by the SORL1 Alzheimer's disease genetic risk factor using human induced pluripotent stem cells. *Cell Stem Cell* **16**, 373-385 (2015).

87. L. K. Fong *et al.*, Full-length amyloid precursor protein regulates lipoprotein metabolism and amyloid-β clearance in human astrocytes. *J Biol Chem* **293**, 11341-11357 (2018).

88. U. Das *et al.*, Activity-induced convergence of APP and BACE-1 in acidic microdomains via an endocytosis-dependent pathway. *Neuron* **79**, 447-460 (2013).

89. G. M. Shankar, A. T. Welzel, J. M. McDonald, D. J. Selkoe, D. M. Walsh, Isolation of low-n amyloid β-protein oligomers from cultured cells, CSF, and brain. *Methods Mol Biol* **670**, 33-44 (2011).

90. K. Johnson-Wood *et al.*, Amyloid precursor protein processing and A beta42 deposition in a transgenic mouse model of Alzheimer disease. *Proc Natl Acad Sci U S A* **94**, 1550-1555 (1997).

91. P. R. Dunkley, P. E. Jarvie, P. J. Robinson, A rapid Percoll gradient procedure for preparation of synaptosomes. *Nat Protoc* **3**, 1718-1728 (2008).

92. L. Fonseca-Ornelas *et al.*, Altered conformation of α-synuclein drives dysfunction of synaptic vesicles in a synaptosomal model of Parkinson's disease. *Cell Rep* **36**, 109333 (2021).

93. H. Wickham, in *Use R!*,. (Springer International Publishing : Imprint: Springer,, Cham, 2016), pp. 1 online resource (XVI, 260 pages 232 illustrations, 140 illustrations in color.

94. H. Wickham. (Journal of Statistical Software, 2007), vol. 21, pp. 1-20.

95. H. Wickham. (Journal of Statistical Software, 2011), vol. 40, pp. 1-29.

FIGURE LEGENDS

Figure 1. Human Aβ42 peptide inhibits γ-secretase-mediated proteolysis of APP_{C99}

(A) The scheme depicts the γ-secretase-mediated cleavage of APP, leading to the generation of Aβ and p3 peptides. In the non-amyloidogenic pathway α-secretase generates a soluble APP ectodomain and a membrane-bound C-terminal fragment of 83 amino acids in length (APP_{C83}), which is then shortened by γ-secretase until a p3 peptide is released. In the amyloidogenic pathway, β-secretase generates a soluble APP ectodomain and a membrane-bound C-terminal fragment of 99 amino acids in length (APP_{C99}), which becomes a substrate for γ-secretase.

The N-terminal sequence of APP_{C99} /Aβ is shown in the lower panel. The differences in the amino acid sequence of human (hu) vs murine (mu) Aβ peptides and the positions of β'- and α-cleavages (that precede the generation of Aβ11-42 and p3 17-42 peptides, respectively) are indicated. The transmembrane domain is labelled in grey and the sequence of Aβ42 is presented within a rectangle.

The initial γ-secretase endopeptidase cut may occur at one of two different positions on APP, generating two different *de novo* substrates that are further processed by carboxypeptidase-like cleavages as follows: Aβ49→Aβ46→Aβ43→Aβ40→Aβ37 or Aβ48 →Aβ45→Aβ42→Aβ38. Aβ38, Aβ40 and Aβ42 peptides are the major products under physiological conditions. The triangles mark the sequential cleavage positions.

(B) The western blot presents AICD products generated *de novo* in detergent-based γ-secretase activity assays using APP_{C99}-3xFLAG at 0.4 μM or 1.2 μM as substrate. To test the inhibitory properties of human Aβ1-42, the peptide was added to the activity assays at concentrations ranging from 0.5 to 10 μM. DMSO at 2.5% was used as a vehicle control. The graphs present the quantification of the western blot bands corresponding to AICDs. The pink and green lines correspond to 0.4 μM and 1.2 μM substrate concentrations, respectively. The data are normalized to the AICD levels generated in the DMSO conditions, considered as 100%. The data are presented as mean ± SEM, N=6-16.

(C) Mass spectrometry-based analysis of *de novo* generated AICD levels in *in vitro* cell-free γ-secretase activity assays containing 3 μM human Aβ1-42 or vehicle (0.6% DMSO) indicate that human Aβ1-42 inhibits both product lines.

(D) The western blot presents *de novo* generated AICDs in detergent-based γ-secretase activity assays using 0.4 μM APP_{C99}-3xFLAG as substrate and wild type γ-secretases composed of different PSEN (1 or 2) and APH1 (A or B) subunits in the presence of vehicle, human Aβ1-42 at 3 μM or GSI (InhX) at 10 μM concentration.

(E) The graph presents ELISA quantification of Aβ1-38 peptides generated in detergent- or detergent resistant membranes (DRM)-based γ-secretase activity assays using either human Aβ1-42 at 10 μM or APP_{C99}-3xFLAG at 1.5 μM as substrates. The data are presented as mean ± SEM, N=3.

(F) The western blot presents *de novo* generated AICDs in detergent-based γ-secretase activity assays using 0.4 μM APP_{C99}-3xFLAG as a substrate and γ-secretase immobilized on sepharose beads. During the first round, the activity assay was supplemented with 3 μM Aβ1-42, 10 μM GSI or DMSO vehicle. After this first round, the γ-secretase-beads were washed to remove the peptide and inhibitor, respectively, fresh substrate was added, and the reaction proceeded for the second round. The analysis demonstrates the reversibility of the Aβ1-42-mediated inhibition.

Figure 2. N- and C-terminus of Aβ influence the inhibitory properties of the peptide

(A, B, C) The western blots present *de novo* generated AICDs in detergent-based γ-secretase activity assays using purified protease and APP_{C99}-3xFLAG at 0.4 μM or 1.2 μM as a substrate. To test the inhibitory properties of (A) murine Aβ1-42, (B) human Aβ11-42 and (C) human p3 17-42, the peptides were added to the assays at concentrations ranging from 0.5 to 10 μM. DMSO at 2.5% was used as a vehicle. The graphs present the quantification of the western blot bands for AICDs. The pink and green lines correspond to 0.4 μM and 1.2 μM substrate concentrations, respectively. The grey dotted lines on the plot B present the curves recorded for human Aβ1-42 (from Figure 1, plot B) for comparison. The data are normalized to the AICD levels generated in the DMSO conditions, considered as 100%, and presented as mean ± SEM, N=3-8.

(D) Detergent-based γ-secretase activity assays using purified protease and APP_{C99}-3xFLAG at 0.4 μM concentration were supplemented with different Aβ peptides at 1 μM concentration or DMSO. *De novo* generated AICDs were quantified by western blotting. The data are shown as mean ± SEM, N=6-27. The statistics were calculated using one-way ANOVA and multiple comparison Dunnett's test, with DMSO (black) or Aβ1-42 (blue) set as references. **p<0.01, **** p<0.0001.

Figure 3. Human Aβ42 inhibits γ-secretase activity in cells

(A) The scheme presents the FRET-based probe allowing monitoring of γ-secretase activity *in situ* in living cells.

(B, C) Spectral FRET analysis of γ-secretase activity in mouse primary neurons using C99 Y-T probe is shown. The cells were treated with the indicated peptides/compounds at 1 μM concentration for 24h. Γ-secretase-mediated proteolysis results in an increase in the distance between two fluorophores incorporated in the probe (YPet and Turquoise-GL). The increase in the distance translates to the reduced FRET efficiency, quantified by the YPet/Turquoise-GL fluorescence ratio. The distribution of recorded FRET efficiency, inversely correlating with γ-secretase activity, is shown in the density plots, N=4 (n=331-354). Medians are shown as dashed lines. Optimal bin number was determined using Freedman-Diaconis rule. The statistics were calculated using Kruskal-Wallis test and multiple comparison Dunn test. Significant differences (*** $p<0.001$) were recorded for DMSO vs Aβ1-42, p3 17-42 vs Aβ1-42, DMSO vs GSI and p3 17-42 vs GSI.

Figure 4. Human Aβ42 leads to the accumulation of APP-CTFs

(A, B, C, F) The western blots present full length APP (APP-FL) and APP C-terminal fragments (APP-CTFs) detected in (A) SH-SY5Y, (B) PC12, (C) ReNcell VM human neural progenitor cells and (F) induced pluripotent stem cell-derived human neurons treated for 24h with respective peptides at indicated concentrations or vehicle (DMSO). The ratio between the APP-CTF and APP-FL levels was calculated from the integrated density of the corresponding western blot bands. The data are shown as mean ± SEM, N=3-23. The statistics were calculated using one-way ANOVA and multiple comparison Dunnett's test, with DMSO set a reference. * $p<0.05$, ** $p<0.01$, **** $p<0.0001$.

(D) The scheme presents the principles of the lactate dehydrogenase (LDH)-based cytotoxicity assay. The figure was created with BioRender.com. Cytotoxicity of the treatments was analyzed in SH-SY5Y cells. The cells were treated with DMSO, Aβ1-42 (1 μM), p3 17-42 (1 μM) or GSI (InhX, 2 μM) for 24h, conditioned medium collected and subjected to the measurement of LDH activity using luminescence-based assay. TX-100 was used as a positive control expected to lead to 100% cell death. The data are shown as mean ± SEM, N=5-17. The statistics were calculated using one-way ANOVA and multiple comparison Dunnett's test, with DMSO set as a reference, **** $p<0.0001$. TX-100 led to a marked increase in the luminescent signal, while no significant toxicity of the other treatments was detected.

(E) The scheme presents the principles of the ATP-based cell viability assay. The figure was created with BioRender.com. Cytotoxicity of the treatments was analyzed in SH-SY5Y cells treated with DMSO, Aβ1-42 (1 μM), p3 17-42 (1 μM) or GSI (Inh X, 2 μM) for 24h. The data are shown as mean ± SEM, N=9-18. The statistics were calculated using one-way ANOVA and multiple comparison Dunnett's test, with DMSO set as a reference. No significant toxicity of the treatments was detected.

(G) Scheme depicts the experimental design testing the impact of biologically-derived Aβ on the proteolysis of APP. Conditioned media were collected from fully differentiated WT human neurons (WT-CM) and human neurons expressing APP with Swedish mutation (SWE-CM). A portion of SWE-CM was subjected to Aβ immunodepletion using the anti-Aβ antibody 3D6. WT, SWE and Aβ immunodepleted (delSWE-CM) CMs were added onto the PC12 cells for 24h to analyze APP processing. As a reference, control cells treated with base media were analyzed. Representative western

blots present the analysis of total cellular proteins from four cell culture sets treated with base media (control), WT-CM, SWE-CM and delSWE-CM, respectively. The ratio between APP-CTFs and APP-FL was calculated from the integrated density of the corresponding western blot bands. The data are shown as mean ± SEM, N=3. The statistics were calculated using one-way ANOVA and multiple comparison Dunnett's test, with control set as a reference, *$p<0.05$.

Figure 5. Human Aβ42 selectively accumulates in the cells and inhibits γ-secretase-mediated proteolysis.

(A) APP-FL and APP-CTF levels in SH-SY5Y cells treated for 24h with a series of Aβ peptides at 1 μM concentration are shown. The APP-CTF/ FL ratio was calculated from the integrated density of the corresponding western blot bands. The data are shown as mean ± SEM, N=3-23. The statistics were calculated using one-way ANOVA and multiple comparison Dunnett's test, with DMSO set as a reference. **** $p<0.0001$.

(B) PC12 cells were treated with respective Aβ or p3 peptides for 24h and stained with anti-Aβ antibody (clone 4G8) followed by anti-mouse Alexa Fluor Plus 488 conjugated secondary antibody, Alexa Fluor Plus 555 conjugated phalloidin and nuclear stain DAPI. Scale bar: 20 μm.

Figure 6. Human Aβ1-42 peptides inhibit proteolysis of multiple γ-secretase substrates.

(A) The western blot presents *de novo* generated NICDs in detergent-based γ-secretase activity assays, using NOTCH1-3xFLAG at 0.4 μM and 1.2 μM as a substrate, supplemented with human Aβ1-42 peptides at concentrations ranging from 0.5 to 10 μM. The graphs present the quantification of the western blot bands for NICDs. The pink and green lines correspond to 0.4 μM and 1.2 μM substrate concentrations, respectively. The data are normalized to the NICD levels generated in the DMSO conditions, considered as 100% and presented as mean ± SEM, N=3-5.

(B) Analysis of the *de novo* ICD generation in cell-free detergent-based γ-secretase activity assays is shown. The graph presents the quantification of the western blots. The data are shown as mean ± SEM, N=3-18. The statistics were calculated using one-way ANOVA and multiple comparison of predefined columns, with Šidák correction test, with respective DMSO supplemented reactions set as a reference, **** $p<0.0001$.

(C) PanCad-FL and PanCad-CTF levels in ReNcell VM cells treated for 24h with human Aβ1-42 peptides at 1 μM or GSI (InhX) at 2 μM concentration were quantified by western blotting. The PanCad-CTF/FL ratio was calculated from the integrated density of the corresponding bands. The data are presented as mean ± SEM, N=6-8. The statistics were calculated using one-way ANOVA and multiple comparison Dunnett's test, with DMSO set as a reference. *$p<0.05$.

(D) PC12 wild type or PC12 deficient for TrkA (PC12nnr5) were incubated with human Aβ1-42 or p3 17-42 peptides, GSI (compound E) or vehicle (DMSO) for 72h. The images present immunocytochemical analyses of cleaved caspase 3, and the graph corresponding quantification of the percentage of cleaved caspase 3 positive cells. The statistics were calculated within PC12 and PC12nnr5 groups using one-way ANOVA and multiple comparison Dunnett's test, with DMSO set as a reference. The data are presented as mean ± SEM, N=3. **$p<0.01$,****$p<0.0001$.

(E) Representative western blot demonstrates the accumulation of p75-CTFs in the cells treated with human Aβ1-42 peptide or GSI. The data are presented as mean ± SEM, N=3. The statistics were calculated within PC12 and PC12nnr5 groups using one-way ANOVA and multiple comparison Dunnett's test, with DMSO set as a reference. *$p<0.05$, **$p<0.01$.

(F) Mouse primary neurons were treated with human Aβ1-42 (1 μM), p3 17-42 (1 μM), GSI (compound E, 10 μM) or vehicle control, in the absence or presence of K252α inhibitor at 0.5 μM. Level of apoptosis in basal frontal cholinergic neurons (BFCNs) was analyzed by immunostaining for choline acetyltransferase (ChAT) and cleaved caspase 3. Representative images are shown. The graph presents the quantification of the percentage of cleaved caspase-3 positive cells among ChAT positive cells. The data are presented as mean ± SEM, N=3. The statistics were calculated within -K252α and +K252α groups using one-way ANOVA and multiple comparison Dunnett's test, with DMSO set as a reference. **p<0.01, ***p<0.001.

Figure 7. Aβ42 does not drastically impact APP-CTF degradation, but have an additive effect to GSI on APP-CTF accumulation.

(A) The scheme presents the experimental design of the cycloheximide (CHX)-based assay evaluating APP-FL and APP-CTF stability.

(B) Western blot shows APP-FL and APP-CTF levels in SH-SY5Y cells at 0, 1, 2.5 and 5h collection points defined in the scheme (A).

(C) The integrated densities of the bands corresponding to APP-FL and APP-CTF were quantified and plotted relatively to the time point zero. The data are presented as mean ± SEM, N=6. Statistics were calculated using two-way ANOVA, followed by multiple comparison Dunnett's test. *$p<0.05$, **$p<0.01$.

(D) Quantification of APP-CTF/ FL ratio at the zero time point is shown. The data are presented as mean ± SEM, N=6. Statistics were calculated using unpaired Student's t-test, **$p<0.01$.

Figure 8. APP-CTFs accumulate in mouse synaptosomes treated with Aβ1-42.

(A) Synaptosomes from brain cortices of three wild type mice were isolated, treated with DMSO or Aβ1-42, and analyzed by western blotting for APP-FL and APP-CTFs. Note the increase in APP-CTF/FL ratio in Aβ1-42 treated samples relative to the control. The data are presented as mean ± SEM, N=3. The statistics were calculated using unpaired Student's t-test. *$p<0.05$.

(B) Schematic representation of the Aβ-driven γ-secretase inhibitory feedback model is shown. Pathological increments in Aβ42 facilitate the establishment of an inhibitory product feedback mechanism that results in impairments in γ-secretase-mediated homeostatic signaling and contributes to AD development. Figure was created with BioRender.com.

Supplementary figure 1. Cell-free γ-secretase activity assay.

Analysis of AICD-3xFLAG levels that are *de novo* generated by purified γ-secretase from the APP_{C99}-3xFLAG substrate is shown. Γ-secretase inhibitor (GSI) and catalytically inactive γ-secretase mutant (DA) were used as negative controls. The left side of the blot presents analysis of unfractionated γ-secretase activity assay samples, while the hydrophilic fraction obtained through methanol:chloroform extraction in presented on the right side. This protein extraction method allows quantification of AICDs without interference of the signal coming from the excess of APP_{C99}-3xFLAG substrate present in the assays. * marks a hydrophobic contaminant.

Supplementary figure 2. Mass spectrometry analysis confirms the inhibitory action of human Aβ1-42 peptides.

The chromatograms present the generation of ICDs from three different substrates in *in vitro* cell-free γ-secretase activity assays, analyzed by mass spectrometry. Solid red – vehicle; dashed red – 3 μM human Aβ1-42.

Supplementary figure 3. Sheddase activation is not behind the APP-CTF accumulation in cells.

(A) The western blots present soluble APP (sAPP) detected in conditioned medium collected from SH-SY5Y cells treated for 24h with respective peptides at 1 μM concentration, GSI (Inh X, 2 μM) or vehicle (DMSO). The sAPP levels were calculated from the integrated density of the corresponding western blot bands. The data are shown as mean ± SEM, N=7-18. The statistics were calculated using one-way ANOVA and multiple comparison Dunnett's test, with DMSO set as a reference. ***$p<0.001$.

(B) The western blots present ADAM10, BACE1, PSEN1-CTF and GAPDH detected in total lysates prepared from SH-SY5Y cells treated for 24h with respective peptides at 1 μM concentration, GSI (InhX, 2 μM) or vehicle (DMSO). The relative expression levels of the proteases were calculated from the integrated density of the corresponding western blot bands and normalized to housekeeping protein levels (GAPDH). The data are shown as mean ± SEM, N=6, with DMSO considered as 100%. The statistics were calculated using two-way ANOVA and multiple comparison Dunnett's test, with DMSO set as a reference. No statistically significant differences were detected between the tested conditions.

Supplementary Tables

Supplementary Table 1. Summary of IC50s in cell-free detergent-based γ-secretase activity assays for selected Aβ peptides.

		IC50 [nM]	
		Substrate: 0.4 µM	**Substrate: 1.2 µM**
AICD	**Aβ1-42**	1259 (N=9)	3565 (N=5)
	Aβ11-42	2218 (N=3)	4685 (N=4)
	p3 17-42	N/A	N/A
	murine Aβ1-42	N/A	N/A
NICD	**Aβ1-42**	609 (N=3)	1564 (N=3)

Figure 1

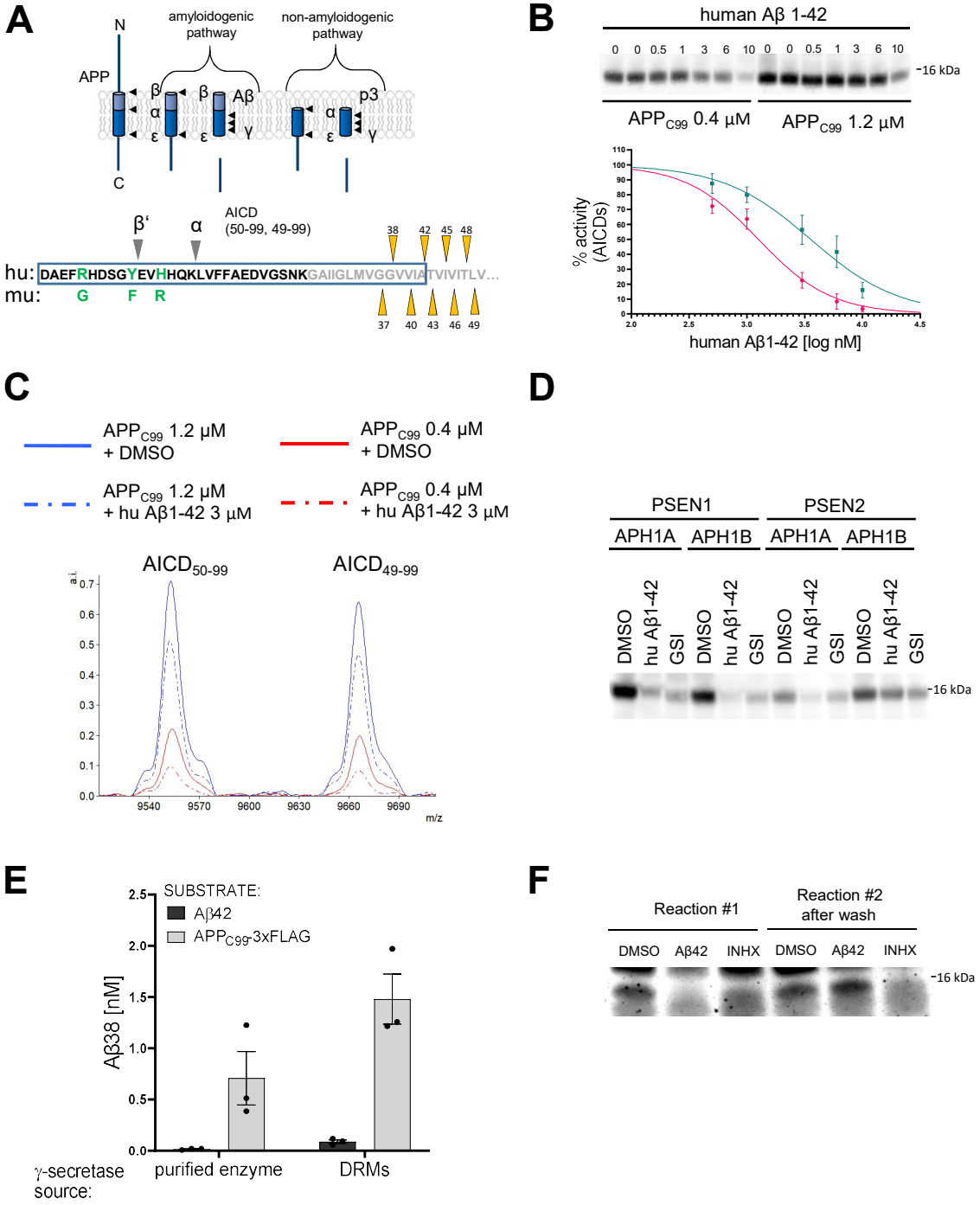

Figure 2

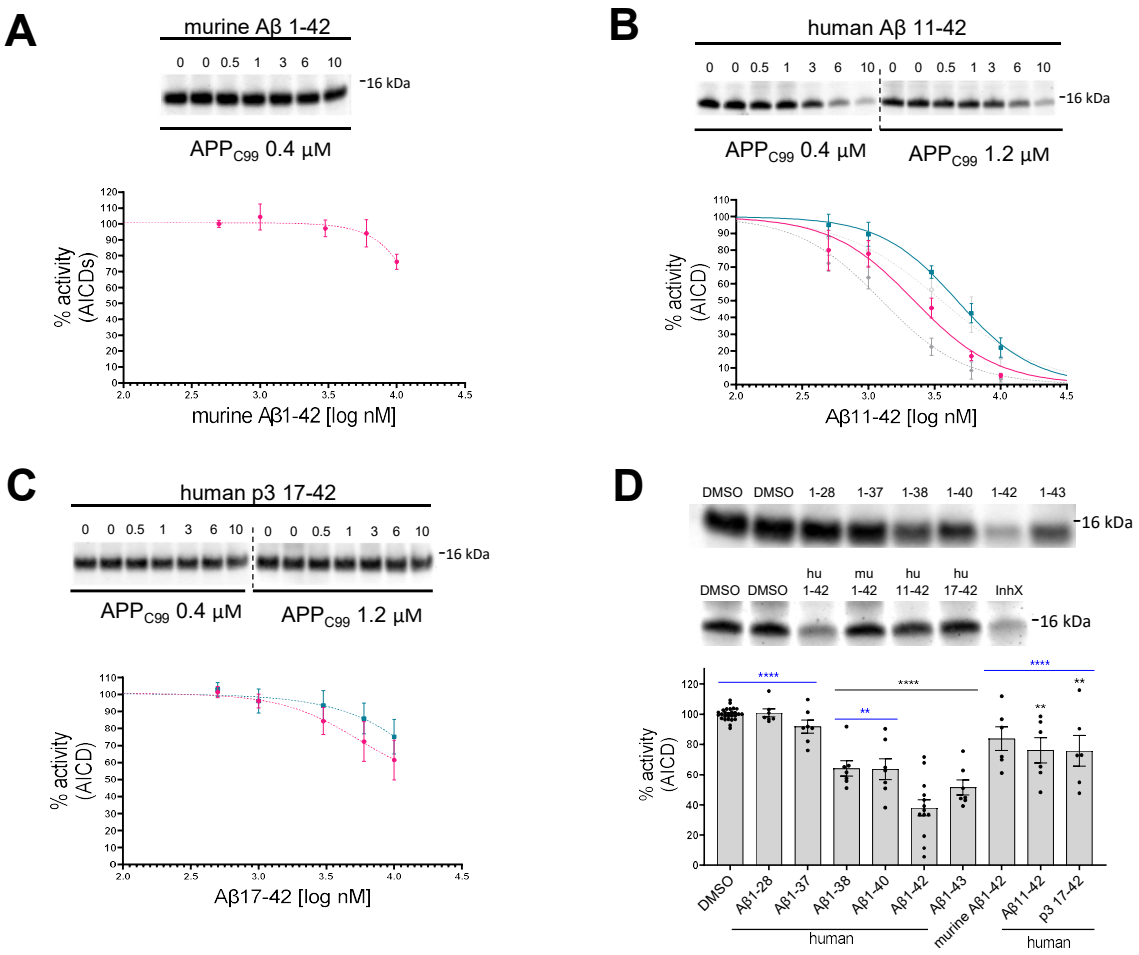

Figure 3

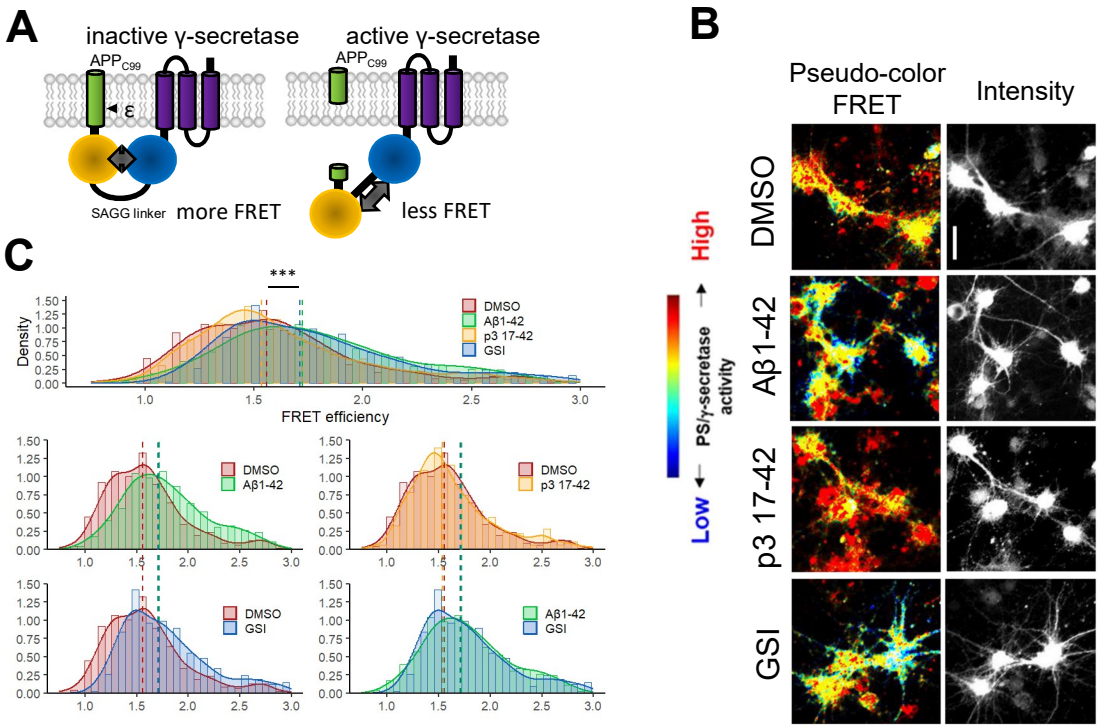

Figure 4

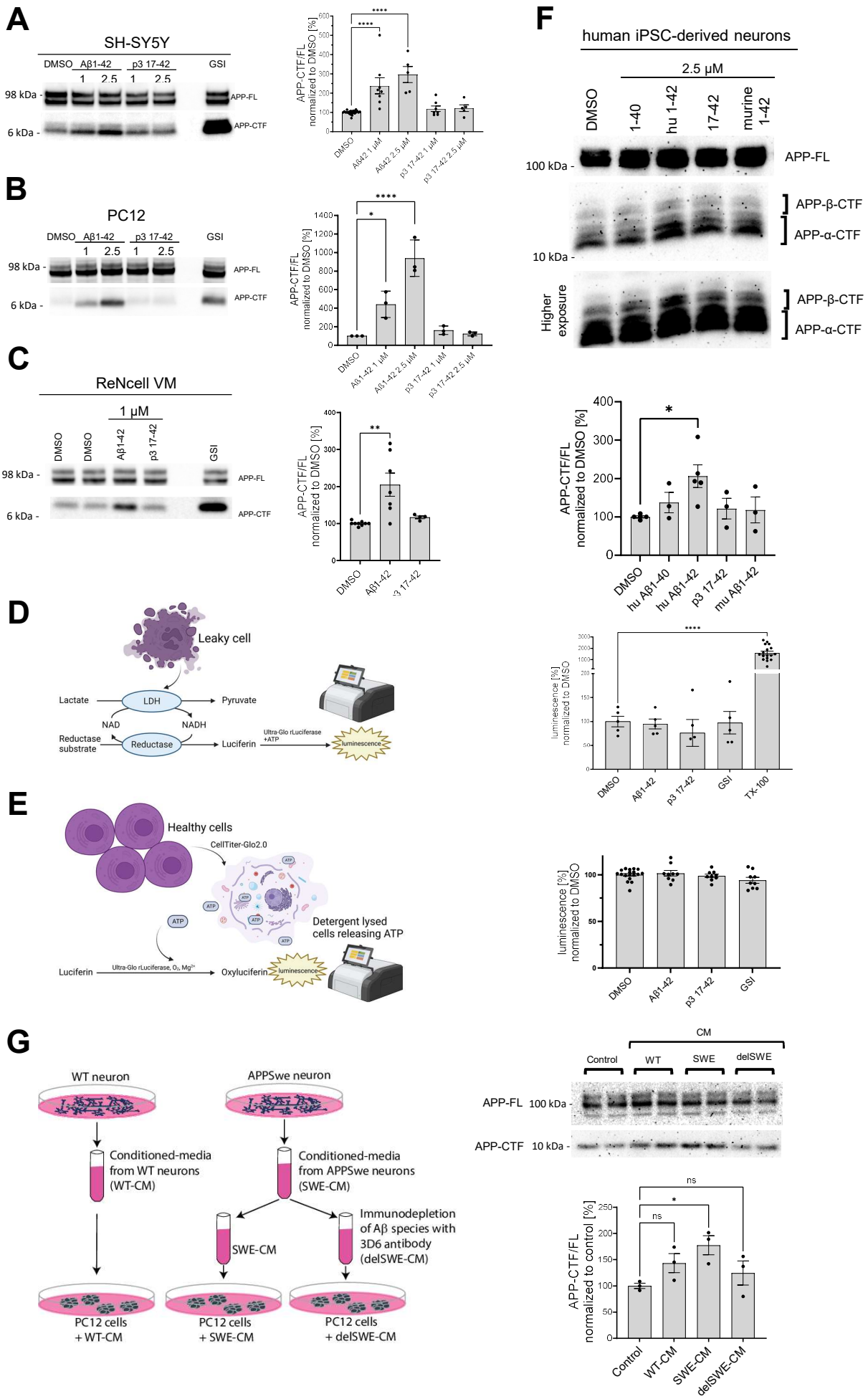

Figure 5

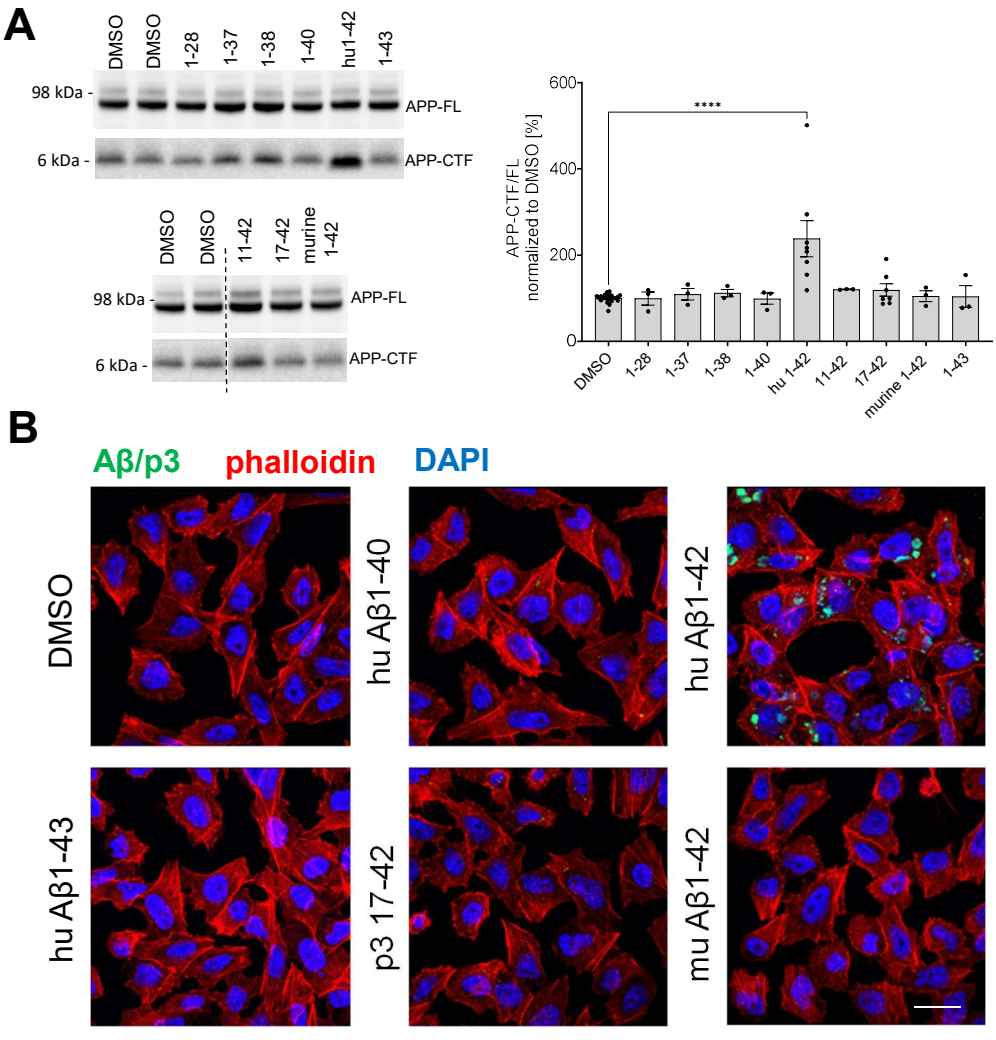

Figure 6

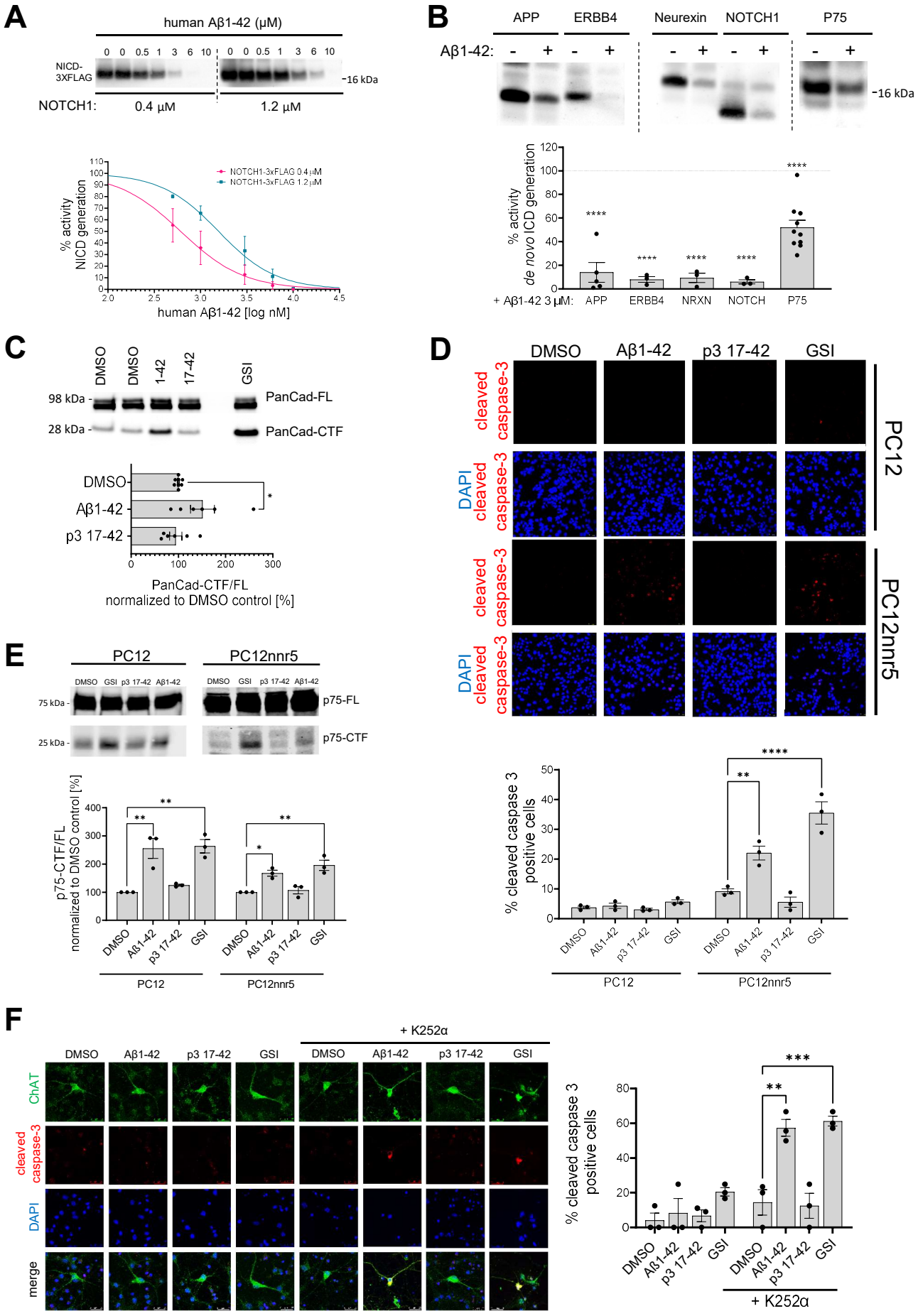

Figure 7

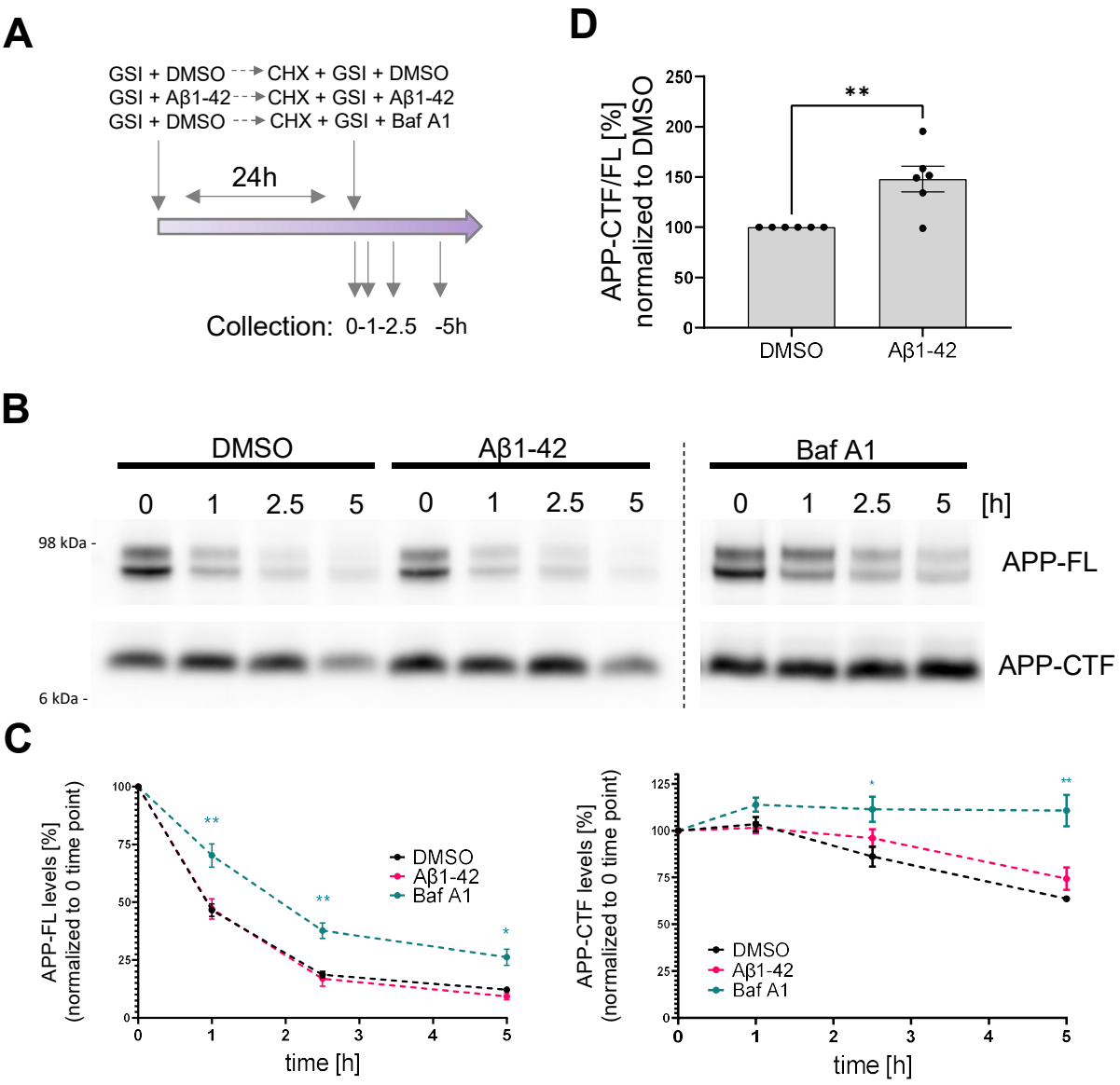

Figure 8

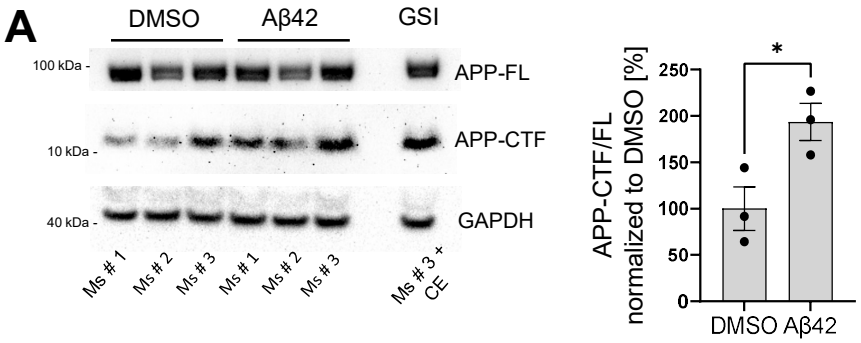

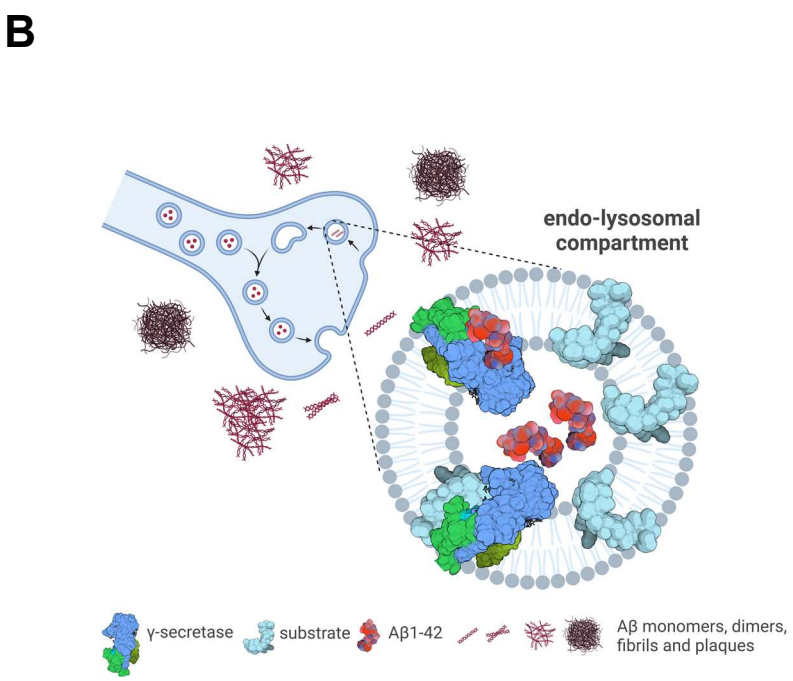

Supplementary figure 1

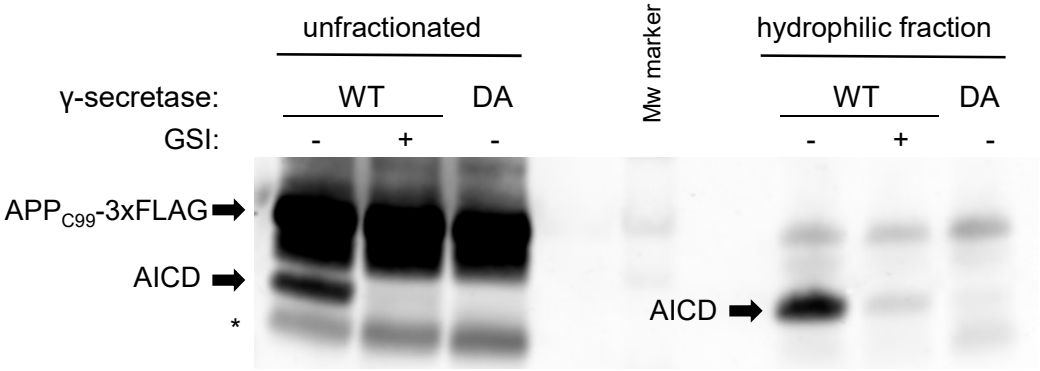

Supplementary figure 2

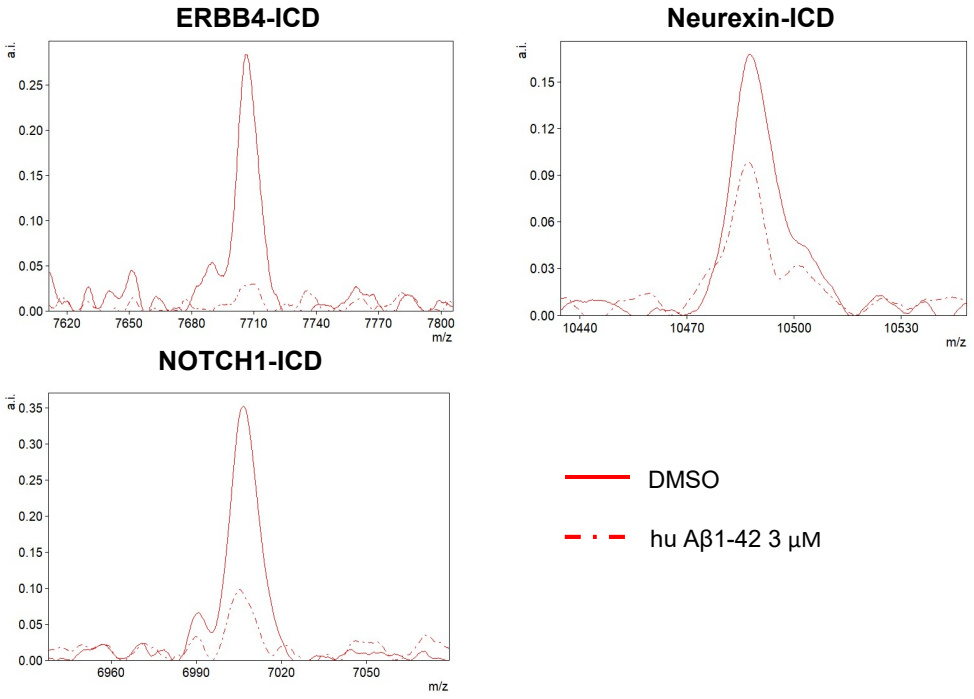

Supplementary figure 3

A

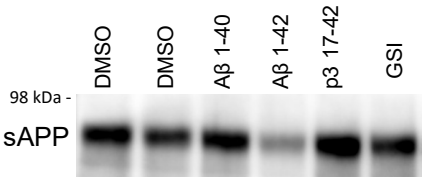

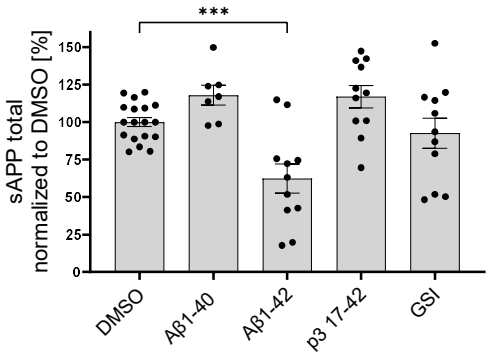

B